

Article

Unlocking Structural Diversity in Gold(III) Hydrides: Unexpected Interplay of cis / trans-Influence on Stability, Insertion Chemistry and NMR Chemical Shifts

Luca Rocchigiani, Julio Fernandez-Cestau, Isabelle Chambrier, Peter Hrobárik, and Manfred Bochmann

J. Am. Chem. Soc., **Just Accepted Manuscript** • DOI: 10.1021/jacs.8b04478 • Publication Date (Web): 04 Jun 2018Downloaded from <http://pubs.acs.org> on June 4, 2018

Just Accepted

“Just Accepted” manuscripts have been peer-reviewed and accepted for publication. They are posted online prior to technical editing, formatting for publication and author proofing. The American Chemical Society provides “Just Accepted” as a service to the research community to expedite the dissemination of scientific material as soon as possible after acceptance. “Just Accepted” manuscripts appear in full in PDF format accompanied by an HTML abstract. “Just Accepted” manuscripts have been fully peer reviewed, but should not be considered the official version of record. They are citable by the Digital Object Identifier (DOI®). “Just Accepted” is an optional service offered to authors. Therefore, the “Just Accepted” Web site may not include all articles that will be published in the journal. After a manuscript is technically edited and formatted, it will be removed from the “Just Accepted” Web site and published as an ASAP article. Note that technical editing may introduce minor changes to the manuscript text and/or graphics which could affect content, and all legal disclaimers and ethical guidelines that apply to the journal pertain. ACS cannot be held responsible for errors or consequences arising from the use of information contained in these “Just Accepted” manuscripts.



Unlocking Structural Diversity in Gold(III) Hydrides: Unexpected Interplay of *cis* / *trans*-Influence on Stability, Insertion Chemistry and NMR Chemical Shifts

Luca Rocchigiani,^{*,†} Julio Fernandez-Cestau,[†] Isabelle Chambrier,[†] Peter Hrobárik,^{*,‡,§} and Manfred Bochmann^{*,†}

[†]School of Chemistry, University of East Anglia, Norwich Research Park, NR4 7TJ, Norwich, United Kingdom

[‡]Institut für Chemie, Technische Universität Berlin, Straße des 17. Juni 135, D-10623 Berlin, Germany

[§]Department of Inorganic Chemistry, Faculty of Natural Sciences, Comenius University, SK-84215 Bratislava, Slovakia

ABSTRACT: The synthesis of new families of stable or at least spectroscopically observable gold(III) hydride complexes is reported, including anionic *cis*-hydrido chloride, hydrido aryl and *cis*-dihydride complexes. Reactions between (C[∧]C)AuCl(PR₃) and LiHBEt₃ afford the first examples of gold(III) phosphino hydrides (C[∧]C)AuH(PR₃) (R = Me, Ph, *p*-tolyl; C[∧]C = 4,4'-di-tert-butylbiphenyl-2,2'-diyl). The X-ray structure of (C[∧]C)AuH(PMe₃) was determined. LiHBEt₃ reacts with (C[∧]C)AuCl(py) to give [(C[∧]C)Au(H)Cl]⁻, whereas (C[∧]C)AuH(PR₃) undergoes phosphine displacement, generating the dihydride [(C[∧]C)AuH₂]. Monohydrido complexes hydroaurate dimethylacetylene dicarboxylate to give *Z*-vinyls. (C[∧]N[∧]C)Au pincer complexes give the first examples of gold(III) bridging hydrides. Stability, reactivity and bonding characteristics of Au(III)-H complexes crucially depend on the interplay between *cis* and *trans*-influence. Remarkably, these new gold(III) hydrides extend the range of observed NMR hydride shifts from δ -8.5 to +7 ppm. Relativistic DFT calculations show that the origin of this wide chemical shift variability as a function of the ligands depends on the different ordering and energy gap between “shielding” Au(d_π)-based orbitals and “deshielding” σ(Au-H)-type MOs, which are mixed to some extent upon inclusion of spin-orbit (SO) coupling. The resulting ¹H hydride shifts correlate linearly with the DFT optimized Au-H distances and Au-H bond covalency. The effect of *cis* ligands follows a nearly inverse ordering to that of *trans* ligands. This study appears to be the first systematic delineation of *cis* ligand influence on M-H NMR shifts and provides the experimental evidence for the dramatic change of the ¹H hydride shifts, including the sign change, upon mutual *cis* and *trans* ligand alternation.

INTRODUCTION

Transition metal hydrides are key components of many catalytic reactions and constitute one of the most important classes of coordination complexes.¹ Hydrides of gold,² by comparison, have been conspicuous by their absence and were long regarded as unstable or hypothetical. The first experimental evidence for their existence was reported by Andrews *et al.* in 2001, who generated binary hydrides such as AuH, (H₂)AuH, (H₂)AuH₃ and [AuH₄]⁻ in frozen gas matrices below 5K.³ The first example of an isolable gold(I) hydride was obtained in 2008, using an *N*-heterocyclic carbene (NHC) as stabilizing ligand.⁴ There are only two types of structurally characterized gold(III) hydrides known so far, both based on stabilization by C[∧]N[∧]C pincer ligands: (C[∧]N[∧]C)AuH (Chart I, structure **A**) first described in 2012,^{5,6} and Bezuidenhout's cation **B**, generated by protonation of the corresponding T-shaped Au(I) bis-carbene complex.⁷ In both cases the hydride ligands are *trans* to N-donors, which exert a weak *trans*-influence and thus increase the Au-H bond enthalpy while reducing its reactivity. The thermally stable hydride **A** was subsequently detected in a number of catalysis-relevant reactions, notably the water-gas shift reaction.^{8,9} Given that gold and hydrogen have very similar electronegativities, Au-H bonds are highly covalent. The reactivity of gold(III) hydrides reflects this; whereas **B** can be deprotonated only by very strong ba-

ses,⁷ complexes of type **A** undergo homolytic Au-H bond cleavage and insertion reactions with alkenes and alkynes via bimolecular pathways involving (C[∧]N[∧]C)Au^{II} radical intermediates.^{6,10}

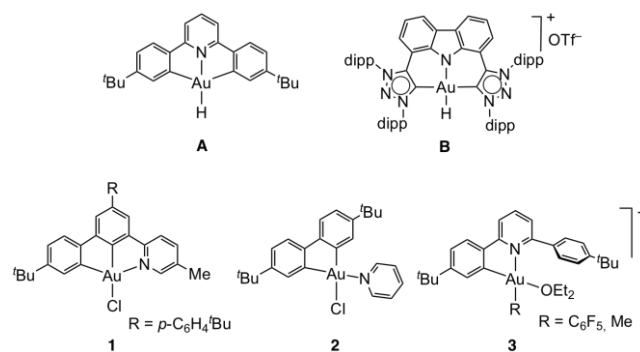


Chart I. Structures of previously reported gold(III) hydrides **A and **B** and of the starting materials **1** - **3**.**

Gold hydrides have been postulated numerous times as part of catalytic cycles and a variety of coordination environments have been assumed,¹¹⁻¹⁴ although experimental evidence for the structural diversity that is accessible to such species is as yet very limited. In square-planar Au(III) complexes the *trans* effect plays a fundamen-

tal role in determining chemical behavior, and the presence of strong electron-donating substituents *trans* to the hydride can dramatically increase the reactivity of the Au-H bond. Some examples in the recent literature showed that *trans*-carbon donors facilitate β -hydride elimination from gold(III) alkyls or formate complexes. Highly reactive gold hydride intermediates were postulated which can undergo insertion or reductive elimination processes.^{11,14} However, until now these types of Au(III) hydrides have not been directly observed.

For this reason, we designed an experimental study aimed at trapping new families of Au(III) hydrides featuring a C-donor in the form of a cyclometalated aryl ligand in *trans* position, in order to investigate analogies and differences with the previously reported hydrides **A** and **B**. To achieve this goal, we explored complexes with different types of ligand environments (Chart I, compounds **1** - **3**). First, we investigated the reactivity of the C[∧]C[∧]N pincer complex **1**¹⁵ towards hydride donors such as LiHBEt₃ at low temperature, with the purpose of observing the corresponding hydride. Second, we extended this strategy to bidentate biphenyl-based C[∧]C chelating ligands (**2**),¹⁶ where the fourth coordination position is occupied by different, non-tethered Lewis bases. Finally, we investigated the C[∧]N chelate complexes **3**, which can be straightforwardly obtained by reacting (C[∧]N[∧]C)Au species with the strong Brønsted acid [H(OEt)₂][H₂N{B(C₆F₅)₃}]₂ (HAB₂). In complexes of type **3**,¹⁷ the dangling aromatic substituent acts as a steric protection for the site *trans* to the cyclometalated aryl group, and this was envisaged to offer the possibility of stabilizing the hydride against reductive elimination.

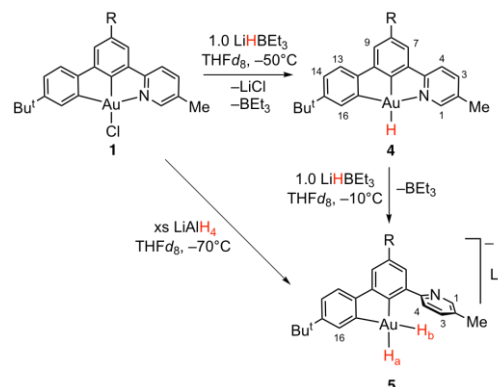
Using the starting materials **1** - **3**, we report here several new classes of gold(III) hydrides, including (i) hydrido phosphine complexes, (ii) anionic hydrides, (iii) dihydrides and (iv) bridging gold(III) hydrides. For the first time it has been possible to synthesize gold(III) complexes with the hydride ligand *trans* to a strong *trans*-effect C-donor ligand. We also show that the coordination geometry has an unexpectedly strong influence on the Au-H ¹H NMR chemical shift, which can cover a range of ~15 ppm. Computational studies show that the ¹H NMR shifts of gold hydrides are strongly influenced by the spin-orbit coupling as a function of the ligand environment and depend on the nature of both *cis* and *trans* ligands. These ligand combinations also affect the thermal stability, leading, for example, to gold(III) phosphine hydrides suitable for crystallographic characterization. The investigation of the reactivity of these new hydrides reveals that they differ distinctly from compounds of type **A**.

RESULTS AND DISCUSSION

(C[∧]C[∧]N) Complexes. C[∧]C[∧]N pincer complexes are coordination isomers of the much more widely studied C[∧]N[∧]C systems^{9,18} and show interesting reactivity and photophysical properties.¹⁵ In bonding terms C[∧]C[∧]N is complementary to C[∧]N[∧]C since strong and weak *trans*-effect ligands have swapped positions and dissociation of the pyridine moiety is less constrained, so that gold(III) hydrides with enhanced reactivity might be expected. With this aim, we explored the reactivity of (C[∧]C[∧]N) gold chloride **1** with 1.0 equivalent of LiHBEt₃ at 198 K. The reaction was monitored by ¹H NMR spectroscopy in THF-*d*₆ gradually raising the temperature from 203 to 243 K. The ¹H NMR spectrum recorded at this temperature showed the clean formation of a single gold-containing species **4**, which retained the typical pattern of a cyclometalated (C[∧]C[∧]N) system (Scheme 1). While no precipitate was seen in

THF, when the reaction was performed in CD₂Cl₂, the formation of solid of LiCl was observed and free BEt₃ was detected in the reaction mixture ($\delta_{\text{B}} = +85.1$ ppm).

Scheme 1. Generation of monohydride **4 and the dihydride **5** (R = *p*-Bu^tC₆H₄), showing the numbering scheme used for NMR assignments.**



Multinuclear and multidimensional NMR experiments performed at 253 K in THF-*d*₆ were consistent with the formulation of **4** as the gold hydride (C[∧]C[∧]N)AuH.¹⁹ The ¹H NMR chemical shifts of metal hydrides are subject to relativistic spin-orbit (SO) effects (“heavy atom effect on the light-atom shielding”, HALA),^{20,21} which in the case of transition metal complexes with *d*⁸ electron configuration are typically shielding,^{20a} as exemplified by shifts of $\delta_{\text{H}} = -6.58$ (CD₂Cl₂) and -8.34 ppm (THF-*d*₆) for **A** and **B**, respectively.^{5,7} In sharp contrast, the signal for the Au-H moiety in **4** is high-frequency shifted at $\delta_{\text{H}} = +6.33$ ppm. An analysis of the dipolar contacts in the ¹H NOESY NMR spectrum revealed selective interactions of the hydride signal with both *ortho*-protons of the coordinated pyridyl and of the cyclometalated aryl, indicating that the pyridine coordination remains intact upon exchange of chloride by hydride. No interactions with BEt₃ groups were observed, excluding the formation of a gold-borohydride Au-HBEt₃ complex. This was further confirmed by diffusion NMR experiments, which showed that **4** and BEt₃ diffuse with different hydrodynamic dimensions. The carbon atom in *trans* position to the hydride is high-frequency shifted compared with the chloride complex and resonates at $\delta_{\text{C}} = 184.2$ ppm; this shift can be attributed to the strong *trans*-influence of the H⁻ ligand and concomitant SO-induced deshielding.^{21,22} On the other hand, the second metalated carbon atom is found at $\delta_{\text{C}} = 145.3$ ppm, being *trans* to the weaker pyridine donor. The NMR peak assignments are also confirmed by relativistic quantum-chemical calculations (cf. Fig. S49 in Supporting Information for ¹³C NMR data) and ¹H hydride shifts are analyzed in detail (see Computational Section below).

In THF solution at room temperature **4** is stable only for a few minutes, hampering its successful crystallization. When an NMR sample was warmed from 253 K to 298 K, broadening of the Au-H and pyridine signals was observed, likely due to pyridine decoordination which may open decomposition pathways. Other solvents, such as benzene-*d*₆ or CD₂Cl₂, can be used for generating **4**, but no improvements in stability were observed. The ¹H NMR signal of the Au-H moiety is marginally affected by the change of solvents and resonates at $\delta_{\text{H}} = 6.99$ and 6.09 ppm in C₆D₆ and CD₂Cl₂, respectively.

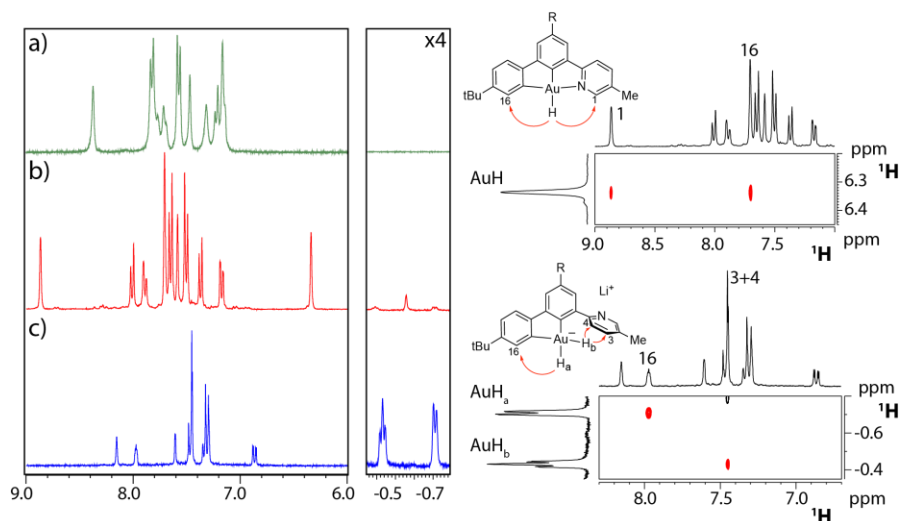


Figure 1. Left: overlay of two sections of the ^1H NMR spectra of (a) **1** (203 K, $\text{THF}-d_6$); (b) **4** (253 K, $\text{THF}-d_6$) and (c) **5** (263 K, $\text{THF}-d_6$). Right: a section of the ^1H NOESY NMR spectrum of **4** (top, 253 K, $\text{THF}-d_6$) and **5** (bottom, 253 K, $\text{THF}-d_6$).

Complex **4** reacts smoothly at room temperature with dimethyl acetylene dicarboxylate (DMAD) under *trans*-hydroauration to give a gold vinyl product (*Z/E*=95:5). A similar vinyl product has previously been obtained by the thermal decomposition of the gold(III) formate complex $(\text{C}^{\wedge}\text{C}^{\wedge}\text{N})\text{AuO}_2\text{CH}$ at 100 °C in the presence of di-*tert*-butyl acetylenedicarboxylate, presumably via **4** as the intermediate.¹⁴ On the other hand, **4** proved unreactive towards unactivated alkynes such as 2-butyne or 1-phenyl-1-propyne. This behavior contrasts with that of hydrides of type **A**, which insert a wide range of alkynes stereoselectively by a radical-mediated outer-sphere mechanism.⁶

When a solution of **4** in $\text{THF}-d_6$ is treated with 1 or more equivalents of LiHBEt_3 at 263 K, the mono-hydride is quantitatively converted into the unprecedented anionic dihydride complex **5**. In striking contrast with what was observed in **4**, both the hydride signals of **5** are shielded and located at $\delta_{\text{H}} = -0.59$ (H_a) and -0.31 ppm (H_b). H_a appears as a doublet with a coupling constant $^2J_{\text{HH}} = 4.2$ Hz, while H_b is a pseudo-triplet due to the simultaneous coupling with H_a and the α proton of the cyclometalated aryl. The assignment of the hydride signals was confirmed by ^1H NOESY spectroscopy, which shows selective dipolar interactions between H_b and the H^3/H^4 pair of the dangling pyridine, while H_a interacts specifically with H^{16} (Figure 1). Both carbon atoms attached to gold are high-frequency shifted due to the high *trans*-influence of the hydride ligands and resonate at $\delta_{\text{C}} = 172.3$ (*C trans* to H_b) and 171.1 ppm (*C trans* to H_a). The dihydride **5** is stable in THF solution for days at room temperature but has so far escaped crystallization. Interestingly, **5** can also be prepared quantitatively by using an excess of LiAlH_4 as hydride transfer agent, with no sign of reduction. The reaction of **5** with DMAD gives a complex mixture, likely arising from possible double insertions and/or vinyl elimination reactions; it did not prove possible to isolate a clean product.

The C[∧]C ligand system. The formation of **5** shows that even anionic gold(III) dihydrides can be made supported by a dianionic C[∧]C chelate backbone, rather than by tridentate pincer ligands. We therefore explored similar ligands which lack the tethered pyridine

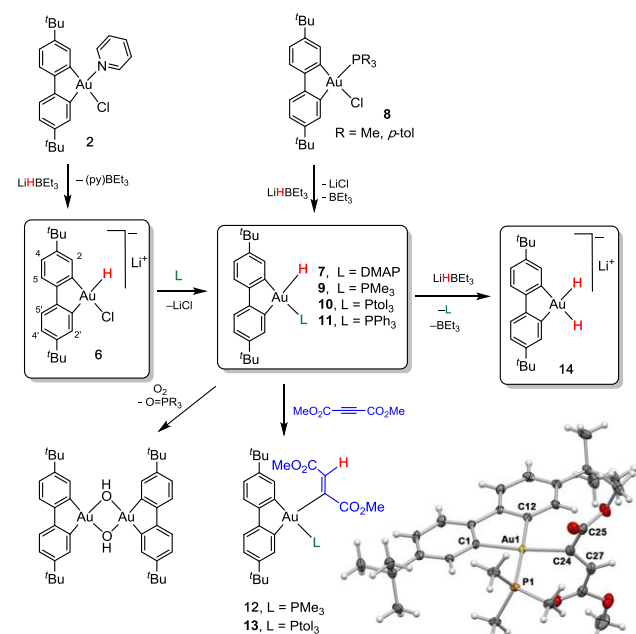
donor. The complex $(\text{C}^{\wedge}\text{C})\text{AuCl}(\text{py})$ **2** ($\text{C}^{\wedge}\text{C} = 4,4'$ -di-*tert*-butylbiphenyl-2,2'-diyl) was combined with 2.0 equivalents of LiHBEt_3 in $\text{THF}-d_6$ at 198 K and the reaction was monitored by ^1H NMR spectroscopy at 223 K. Soon after mixing the reagents, the solution turned bright yellow, and the first NMR spectrum showed the complete consumption of the starting material to give a single clean species showing two different sets of signals for the C[∧]C ligand, suggesting the formation of an asymmetric gold complex. ^1H NOE and diffusion NMR spectroscopy showed that the $\text{py} \rightarrow \text{BEt}_3$ Lewis adduct had formed. The data are consistent with pyridine displacement by the hydroborate and elimination of the borane-pyridine adduct, leading to the formation of the chloro hydride anion, $[(\text{C}^{\wedge}\text{C})\text{Au}(\text{H})\text{Cl}]^-$ (**6**). The reaction of **2** is therefore quite different from that of the $(\text{C}^{\wedge}\text{C}^{\wedge}\text{N})$ ligand system **1**, where the pyridine was not initially displaced. The Au–H moiety in **6** was identified as a broad singlet at $\delta_{\text{H}} = +2.43$ ppm, which showed selective dipolar interactions with only one α proton of the ligand at $\delta_{\text{H}} = 7.72$ ppm. As observed for **4**, the two metalated carbon atoms resonate at quite different frequencies, due to the different *trans*-influences of the chloride and hydride ligands, such that *C trans* to H resonates at $\delta_{\text{C}} = 174.8$ ppm, while *C trans* to Cl is found at 148.4 ppm. Product **6** is stable in solution for hours at 213 K, but upon raising the temperature to 253 K it is converted to an undefined secondary species showing a broad hydride signal at $\delta_{\text{H}} = +0.9$ ppm. Diffusion NMR experiments in CD_2Cl_2 at 228 K suggested the formation of aggregates containing at least four gold centers. This species undergoes reductive decomposition above 253 K, and its identity could not be ascertained. Since this reactivity was likely due to the facile chloride elimination from **6**, we explored more strongly coordinating bases to stabilize the hydride products.

In order to intercept a $(\text{C}^{\wedge}\text{C})\text{Au}$ hydride of a structure comparable to **4**, the chloro hydride **6** was reacted with 1 molar equivalent of *p*-dimethylaminopyridine (DMAP) at 195 K and the resulting mixture was monitored by ^1H NMR spectroscopy at 253 K. Although at a 1:1 stoichiometry DMAP does not bind to gold but displaces pyridine from the $\text{py} \rightarrow \text{BEt}_3$ adduct, with 4.0 equivalents of

DMAP **6** is converted quantitatively to (C[^]C)AuH(DMAP) (**7**) (Scheme 2). This complex shows a hydride signal at $\delta_{\text{H}} = +3.25$ ppm, which exhibits NOE interactions with one α proton of the C[^]C ligand and with the *ortho* protons of the coordinated DMAP ($\delta_{\text{H}} = 8.10$). ¹H NOESY NMR reveals that at 253 K free and coordinated DMAP are in chemical exchange. Likely for this reason, **7** decomposes at room temperature within about 30 minutes.

By contrast, thermally stable hydrides are straightforwardly obtained by reacting the phosphine complexes (C[^]C)Au(Cl)PR₃ **8** (R = Me, *p*-tolyl) with LiHBEt₃ in toluene at room temperature to give spectroscopically clean samples of **9** and **10**, respectively, which were isolated by filtration and vacuum drying. The same complexes, as well as the PPh₃ derivative **11**, are also accessible from the chloro hydride **6** on reaction with phosphines. However, in that case purification and crystallization of the products was hampered by the presence of the py \rightarrow BEt₃ by-product, which displays similar solubility characteristics to **9**–**11** in organic solvents.

Scheme 2. Synthesis and reactions of (C[^]C)gold(III) hydrides, showing the atom numbering scheme used for NMR assignments, and the molecular structure of the insertion product **12^a**



^aSelected bond distances [Å] and angles [°]: Au1-C1 2.079(7), Au1-C12 2.070(6), Au1-P1 2.353(2), Au1-C24 2.078(7), C1-Au1-C12 81.1(3), C1-Au1-P1 96.8(2), P1-Au1-C24 89.7(2), C24-Au1-C12 92.3(3), C1-Au1-C24 173.4(3), C12-Au1-P1 177.3(2), torsion C1-Au1-C24-C25 91(2), torsion C1-Au1-C24-C27 -88(3).

The complexes **9**–**11** are stable in THF solution at room temperature for several days. The ³¹P NMR spectra showed high-frequency shifted signals at $\delta_{\text{P}} = -8.2$, $\delta_{\text{P}} = 32.6$ and $\delta_{\text{P}} = 34.9$ for **9**, **10** and **11**, respectively, confirming phosphine coordination. The ¹H NMR hydride signals at 1.53 (**9**), 2.33 ppm (**10**) and 2.40 (**11**) and appear as doublets due to their coupling with the phosphorus atoms. The ²J_{PH} values (32.6 Hz for **9**, 33.0 for **10** and 32.3 Hz for **11**) are compatible with H and P in *cis*-positions. ²J_{PC} values are in agreement with the proposed structures: *trans* couplings fall between 130 and 140 Hz, while *cis* ²J_{PC} constants are about 4–5 Hz.

Single crystals of **9** were obtained by the slow evaporation of a dry diethyl ether solution under an N₂ atmosphere. The structure

contains four independent molecules in the asymmetric unit, with very similar structural parameters. Figure 2 gives the geometric parameters of just one of these molecules. A complete description of the structure is given in the Supporting Information. Locating the position of the hydride next to a heavy atom correctly by crystallography is intrinsically difficult; however, the Fourier map for the Au coordination plane unequivocally reveals the presence of electron density at a distance of about 1.4 Å (see Supporting Information, Figure S45). The other structural parameters are as expected for a square planar Au(III) complex. From the differences between the two Au-C bonds of the C[^]C ligand, the hydride exerts a larger *trans* influence than the phosphine (Au1-C1 2.047(4) Å vs. Au1-C12 2.115(4) Å).

Although solid samples of **9**–**11** are thermally stable under ambient conditions, crystallization attempts of **9** in toluene also revealed that over time reductive C-H elimination and ligand rearrangements are possible, as indicated by the isolation of the gold(I) complex [(tBuC₆H₃)₂(AuPMe₃)₂]_x as a by-product (see Supporting Information, Figure S46). Furthermore, unlike the (C[^]N[^]C)AuH hydrides of type **A** which are stable to air, moisture and weak acids, solutions of **9**–**11** are sensitive to exposure to air. For example, a sample of **10** left to crystallize without a protective atmosphere afforded the crystallographically identified hydroxide [(C[^]C)Au(μ-OH)]₂, together with (*p*-tol)₃P=O (see SI, Figure S47). The formation of these products suggests O₂ insertion into the Au-H bond²³ to give an Au(OOH)(PR₃) intermediate, which decomposes to the gold hydroxide with oxidation of the phosphine. This reactivity was also observed upon reacting **10** with dry O₂.

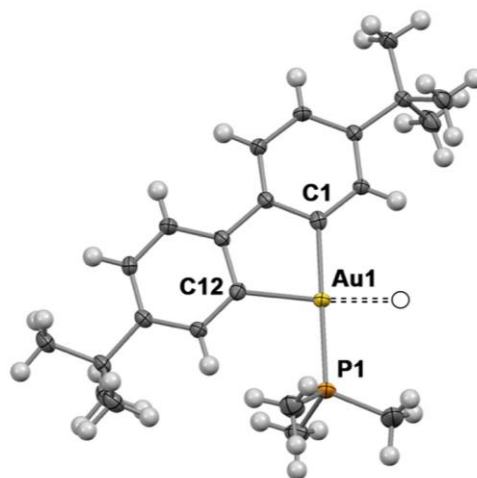


Figure 2. Molecular structure of (C[^]C)AuH(PMe₃) **9**; the approximate hydride position is indicated by an open circle. Selected bond distances [Å] and angles [°]: Au1-C1 2.047(4), Au1-C12 2.115(4), Au1-P1 2.325(1), C1-Au1-C12 81.5(2), C12-Au1-P1 98.7(1), C1-Au1-P1 179.6(1).

As in the case of **4**, the hydrides **9** and **10** insert DMAD to give the corresponding *Z*-vinyl complexes **12** and **13**. However, whereas **4** reacts instantaneously with DMAD at room temperature, the same reaction with **9** and **10** proceeds more slowly. When 1–2 molar equivalents of DMAD are used, **9** is consumed within 2 h, while the reaction of **10** takes about 12 h, likely due to the increased steric repulsion of the phosphine ligands. The reaction affording **12** is quantitative, whereas **13** is formed in 80% yield together with unidentified side products.

The stereochemistry of the DMAD hydroauration products was proved by ^1H NOE NMR spectroscopy, which showed the presence of dipolar contacts between the vinylic CH and both the methoxy groups. No signs of *Z/E* isomerization were observed after 2 days in solution. Single crystals of **12** suitable for X-ray diffraction were obtained by slow evaporation of a toluene/dichloromethane solution. The crystal structure confirmed the *trans*-orientation of the two methylcarboxylate moieties. The vinyl group adopts a perpendicular orientation with respect to the coordination plane of Au (torsion angle C1-Au1-C24-C27 $88(3)^\circ$). The planar disposition of the C28(O)OMe carboxylate group and the vinyl moiety is indicative of π -delocalization; the other carboxylate residue adopts a twisted geometry. The orientation of the carboxylate groups is stabilized in the solid state by a network of intermolecular O...H interactions.

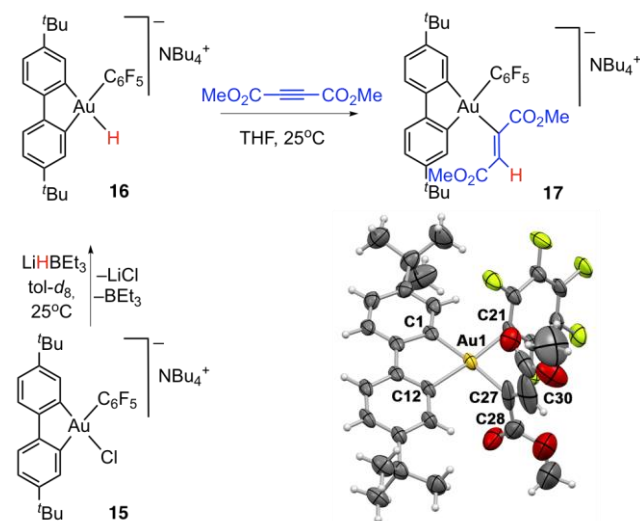
The addition of a second molar equivalent of LiHBEt_3 to **9** and **10** leads to the substitution of the phosphine ligand by H, to give the anionic *cis*-dihydride **14** (Scheme 2). For example, upon reacting **10** with 1.0 equiv LiHBEt_3 at room temperature in THF- d_6 , ^{31}P NMR spectroscopy revealed the disappearance of the signal at $\delta_{\text{P}} = 32.6$ and the concomitant formation of free *para*-tolyl phosphine ($\delta_{\text{P}} = -8.0$). The ^1H NMR spectrum indicated a C_2 -symmetric C \wedge C ligand, together with a new signal at $\delta_{\text{H}} = 0.09$ which accounts for two protons and is assigned to Au-H (Supporting Information, Figures S23-S24). The hydride signal appears as a pseudo-triplet, due to coupling with the two C \wedge C ring protons in 2 and 2' positions; these protons also show selective NOE interactions with the hydride signal. In agreement with these observations, the Au-C carbon atoms resonate at $\delta_{\text{C}} = 170.7$ in the ^{13}C NMR spectrum. Complex **14** can be also generated in toluene- d_8 , for which the hydride resonance of the AuH $_2$ moiety was found at $\delta_{\text{H}} = 1.00$ ppm. Given that for *cis*-(Ph $_3$ P)AuClH(Ph) and *cis*-(Ph $_3$ P)AuClH $_2$ the calculated barriers for C-H reductive elimination are only 7.5 and 6.5 kcal mol $^{-1}$, respectively, 24 and considering the lack of orbital directionality of H, the observed thermal stability of gold(III) hydrido aryls **9** – **11** and of the dihydride **14** is remarkable and unexpected. As was seen for **10**, eventually reductive decomposition does take place, and although **14** appears stable at room temperature for hours in THF and toluene solutions, any isolation attempts led to reductive decomposition, affording free biphenyl and metallic gold.

Other gold *cis*-hydrido aryl complexes resistant to reductive elimination are similarly accessible, by treatment of the pentafluorophenyl complex $[\text{NBu}_4]^+[(\text{C}\wedge\text{C})\text{Au}(\text{Cl})\text{C}_6\text{F}_5]$ (**15**) at room temperature with 1.2 equiv LiHBEt_3 . The anionic hydride **16** is formed in quantitative yield, according to ^1H NMR spectroscopy (Scheme 3). The chloride-to-hydride exchange in THF- d_6 is comparatively slow and complete within 24 h, whereas in toluene the formation of **16** is instantaneous. The Au-H signal resonates at $\delta_{\text{H}} = 1.15$ ppm in THF- d_6 , partially overlapping with a *tert*-butyl signal, and was identified by means of its selective dipolar interaction with the H 2 proton of the cyclometalated aryl ring at $\delta_{\text{H}} = 8.06$ ppm. As was seen previously for neutral C \wedge C hydrides, the cyclometalated carbon atom *trans* to the hydride is high-frequency shifted to $\delta_{\text{C}} = 170.3$, while the one *trans* to C $_6\text{F}_5$ resonates at $\delta_{\text{C}} = 160.1$ ppm. Complex **16** reacts readily with DMAD to give the corresponding *trans*-vinyl complex **17**. In contrast with the phosphine hydrides **9** and **10**, the reaction with **16** is instantaneous at room temperature. The stereochemistry was confirmed by ^1H NOESY NMR spectroscopy

and by single crystal X-ray diffraction of **17** (Scheme 3). The structural parameters of the anionic vinyl **17** are very similar to those found for **12**.

While phosphine dissociation and creation of a coordination site *cis* to the hydride could in principle be considered a possible pathway in the reactions of phosphine hydrides **9** and **10** with DMAD, the facile alkyne insertion into the Au-H bond of **16**, where no such ligand dissociation is possible, shows that alkyne π -coordination to Au(III)-H is not part of the insertion process. We also established that, unlike the insertion reactions of (C \wedge N \wedge C)AuH (**A**) with alkyl and aryl acetylenes, 6 a radical chain reaction via Au(II) intermediates is not involved.

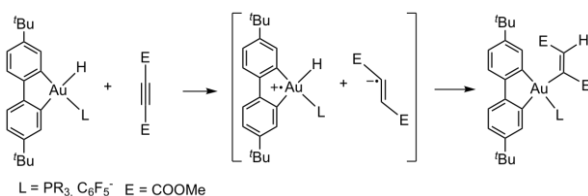
Scheme 3. Synthesis of $[\text{NBu}_4]^+[(\text{C}\wedge\text{C})\text{AuH}(\text{C}_6\text{F}_5)]$ (16**) and the formation and molecular structure of the alkyne insertion product **17** (NBu_4^+ omitted for clarity). a**



a Selected bond distances [Å] and angles [$^\circ$]: Au1-C1 2.046(8), Au1-C12 2.063(6), Au1-C27 2.093(8), Au1-C21 2.088(6), C27-C28 1.57(2), C27-C30 1.22(2), C1-Au1-C12 80.8(3), C1-Au1-C21 93.7(3), C21-Au1-C27 89.9(3), C27-Au1-C12 95.7(3), C1-Au1-C27 174.4(3), C12-Au1-C21 174.4(3).

While a detailed study of this insertion mechanism is beyond the scope of this work, it is apparent that only alkynes with a low reduction potential insert into the gold hydrides described here. A similar observation was made with the gold(I) hydride (IPr)AuH (IPr = 1,3-bis(*diisopropylphenyl*)imidazol-2-ylidene). 4 DMAD has a reduction potential of only -0.8 V (compared to a value of -2.1 V for diphenylacetylene). 25 It seems likely therefore that the insertion of DMAD follows an electron transfer mechanism, which would generate an alkyne radical anion within the solvent cage. Alkyne radical anions are known to exhibit *trans* geometry, 26 and such an intermediate, followed by H abstraction and Au-C bond formation, would explain the observed *Z*-vinyl stereochemistry of DMAD hydroauration (Scheme 4). The reactivity of our gold(III) hydrides seems to resemble therefore the DMAD insertion process observed for platinum dihydrides *trans*-H $_2$ Pt(PR $_3$) $_2$ (but *not* for *trans*-PtH(Cl)(PEt $_3$) $_2$, which follows a coordination-*cis* insertion pathway). 27

Scheme 4. Proposed mechanism of DMAD hydroauration with (C[∧]C)Au hydrides.

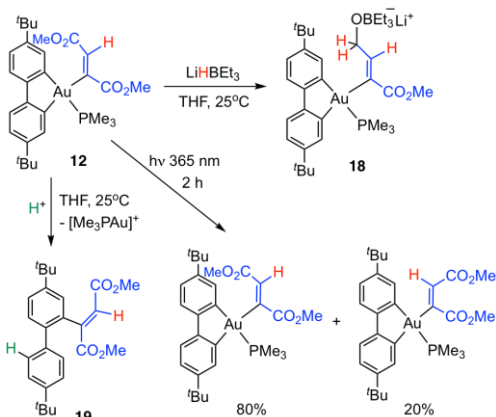


Reactivity of (C[∧]C)gold vinyl complexes. As we observed previously, (C[∧]N[∧]C)Au(III) vinyl complexes obtained by alkyne *trans*-hydroauration are thermally stable and are not protodeaured by strong acids.⁶ This might be ascribed to the effect of the weak pyridine donor *trans* to vinyl, which strengthens the Au–C bond. In **12**, **13** and **17**, the vinyl ligands are *trans* to anionic carbon, which exerts a much stronger *trans* effect and thus labilize the Au–vinyl bond. In order to investigate whether this structural modification has an impact on the reactivity of these complexes, we explored photoisomerization, protodeauration and reduction with LiHBET₃ of these gold vinyls.

Photoisomerization of **12** and **17** was performed by irradiating samples in THF-*d*₈ at 365 nm for 2 hours at room temperature. **12** does not photoisomerize easily under these conditions and gives a thermodynamic *E/Z* ratio of 20:80, whereas the anionic vinyl complex **17** leads to an equilibrium *E/Z* ratio of 50:50. This supports the hypothesis that the *Z* isomer obtained upon hydroauration of DMAD is the kinetic product and that the structure of the ancillary ligand has an impact on the isomer distribution in the thermodynamic mixture.

The reactivity of (C[∧]C)Au vinyl complexes towards acids and hydrides was exemplified for **12**. On treatment with 2.5 equivalents of LiHBET₃, **12** reacts quantitatively under selective reduction of one of the two ester functions to give the alkoxyvinyl product **18** (Scheme 5). The identity of **18** was confirmed by multinuclear and multidimensional NMR spectroscopy (Supporting information). This reactivity demonstrates the facile post-synthesis derivatization of alkyne hydroauration products and their remarkable resistance to reducing conditions.

Scheme 5. Photoisomerization, ester reduction and reductive C–C bond formation of gold vinyl complexes.



Reductive elimination of a C–C cross-coupling product can be induced by acids. When a solution of **12** in THF-*d*₈ was treated with the strong Brønsted acid [H(OEt₂)] [H₂N{B(C₆F₅)₃}₂]²⁸ (1 equiv) at room temperature, the orange color of the solution faded

immediately and a dark precipitate of metallic gold was observed. The ¹H NMR spectrum of the supernatant revealed the formation of the 2-vinylbiphenyl **19** in about 65% yield. Protodeauration of the Au–vinyl bond to give MeO₂CH=CHCO₂Me was not detected. The appearance of an AB system at δ_H = 7.20 and 7.34 ppm suggests that the acid protodeaures selectively one Au–C bond of the cyclometalated C[∧]C ligand, likely *trans* to vinyl, to give a cationic aryl–vinyl intermediate capable of reductive C–C coupling. This Au–aryl bond cleavage kinetically outperforms Au–vinyl protonation. The stereochemistry of the vinyl group is retained in **19**.

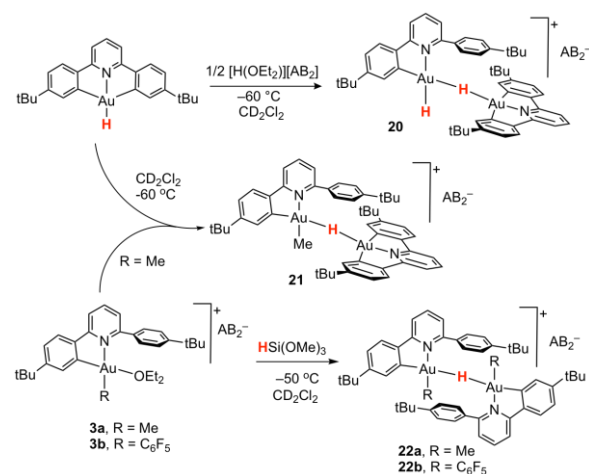
The C[∧]N–CH ligand system. Protodeauration of (C[∧]N[∧]C)Au(III) pincer complexes with HAB₂ affords cleaved (C[∧]N–CH)Au(III) cations **3** (Scheme 6), where a Et₂O molecule is weakly coordinated to gold in *trans* position to the remaining cyclometalated aryl.¹⁷ We therefore envisioned that this particular ligand environment could offer the possibility to intercept yet another family of Au(III) hydrides which could also have the hydride ligand *trans* to a carbon atom but, being supported by a C[∧]N rather than a C[∧]C chelate, would constitute the cationic analogues of the (C[∧]C)AuH(L) species described above. Moreover, the presence of the dangling aryl group might offer extra steric protection to the hydride moiety.

As a first control experiment, we re-investigated the reaction of (C[∧]N[∧]C)AuH with HAB₂ at a 1:1 molar ratio. As previously reported, the Au–H bonds in pincer gold(III) hydrides are covalent and do not liberate H₂ upon reaction with acids. Instead, one Au–C bond is protolytically cleaved, a process that can be expected to enable fast reductive C–H elimination.²⁹ To our surprise, when the protodeauration reaction was performed at 213 K in CD₂Cl₂, the starting material was quantitatively converted to the new species **20**. This complex shows two scalarly coupled hydride signals, both at much lower frequency than the ones seen for C[∧]C complexes, δ_H = -4.88 and δ_H = -8.39 ppm. In the aromatic region of the ¹H NMR spectrum there are two sets of signals in a 1:1 ratio, with one set showing the typical fingerprint of a cleaved (C[∧]N–CH) ligand, while the second set was that of an intact (C[∧]N[∧]C)Au fragment. In agreement with this, only 50% of the added acid had in fact reacted, with the other 50% remaining unchanged (δ_H = 16.7 ppm). These findings were consistent with protodeauration of one pincer Au–C bond to generate a cationic gold hydride, followed by coordination of a molecule of neutral (C[∧]N[∧]C)AuH to the vacant coordination site on the [(C[∧]N–CH)AuH]⁺ cation to give the H-bridged binuclear dihydride **20** (Scheme 6). Whereas in gold(I) chemistry H-bridged complexes are not uncommon,⁴ this is the first example of a bridging hydride in gold(III) chemistry. In agreement with the reaction sequence outlined above, the same product can be generated using only 0.5 equivalents of acid. The geminal coupling constants for the dihydride was found to be 8.2 Hz, much larger than the geminal coupling in the anionic mononuclear dihydride **6** (²J_{HH} = 4.2 Hz). ¹H NOESY methods allowed us to assign the signals at δ_H = -4.88 and δ_H = -8.39 ppm to the bridging and the terminal hydride, respectively. Unfortunately, the dihydride **20** is thermally unstable and at 213 K decomposes over a period of 1 hour, hampering full ¹³C NMR characterization.

In analogy to complex **20**, the cationic gold(III) methyl complex **3a** reacts with 1 equivalent of (C[∧]N[∧]C)AuH at 213 K to give the bridging hydride **21** (δ_H = -5.14 ppm). Product **21** proved to be rather unstable and decomposed at low temperature within hours, in line with the low barrier of reductive methane elimination calcu-

lated for $(\text{Ph}_3\text{P})\text{AuH}(\text{CH}_3)\text{Cl}$ (11.1 kcal mol⁻¹).²⁴ Nevertheless, it seems remarkable that gold hydrido methyl complexes are so readily accessible.

Scheme 6. Formation of binuclear C[∧]N bonded gold(III) hydrides



In the search for milder hydride donors, the reactions of the cleaved pincer complexes **3a** and **3b** with $\text{HSi}(\text{OMe})_3$ were tested. Complexes **22a** ($\text{R} = \text{Me}$) and **22b** ($\text{R} = \text{C}_6\text{F}_5$) proved to be more stable than **20** and **21** and could be fully characterized by multinuclear NMR at low temperature. The hydride signal appeared as singlets at $\delta_{\text{H}} = -2.53$ and $\delta_{\text{H}} = -2.21$ ppm for **22a** and **22b**, respectively (Supporting Information, Figure S41). The ¹H NMR spectra of complexes **22a, b** show the presence of four different signals for the dangling aryl substituents, suggesting that dimerization of two gold units blocks the free rotation of the aromatic ring about the C–C bond. ¹H NOESY NMR spectroscopy revealed the presence of selective dipolar interactions between the bridging hydride and only one proton of the protodeaured ring, confirming that the Au–H–Au moiety is located in the pocket formed by the two paired cleaved pincer complexes. In the case of complex **22a**, the same interaction was observed for the Au–Me moiety.

Although complexes **22a, b** are stable at 253 K, they decompose at room temperature, following reaction pathways which depend on the substituents on gold. Warming a sample of **22b** to 297 K generates $\text{C}_6\text{F}_5\text{H}$ quantitatively within minutes; in this case the reductive coupling of H with C_6F_5 is preferred. The methyl complex **22a** is slightly more thermally stable and survives 297 K for about 30 minutes before decomposing. However, there is *no* elimination of CH_4 ; instead, the methyl migrates to the C[∧]N[∧]C ligand, while the hydride is likely eliminated through reductive deprotonation to give protonated pyridinium salts.³⁰

Connection between gold hydride ¹H NMR chemical shifts and electronic structure. The gold(III) hydride complexes described above are characterized by a spread of ¹H NMR chemical shifts covering an unexpectedly wide range of about 15 ppm. Table 1 summarizes the relevant structural, calculated and experimental data. Particularly striking is the difference between the regioisomeric pincer complexes (C[∧]N[∧]C)AuH and (C[∧]C[∧]N)AuH, which show resonances of $\delta = -6.51$ and $+6.09$ ppm, respectively (both in CD_2Cl_2). While the former features an upfield (low-frequency) shift often seen for diamagnetic hydride complexes with a partially filled d-shell,¹⁹ the latter displays a notable downfield ¹H shift, resembling that in a gold(I) hydride, $(\text{IPr})\text{AuH}$,⁴ although both (C[∧]N[∧]C)AuH and (C[∧]C[∧]N)AuH contain the metal center in the

same +III oxidation state. To rationalize the observed trends and to gain insight into the electronic structures and the factors that result in these spectroscopic differences, we turned to relativistic quantum-chemical calculations of structures and ¹H NMR hydride shifts at the two-component ZORA-SO level, including spin-orbit coupling (see Supporting Information for Computational details).^{31,32}

All investigated structures were optimized at the PBE0-D3(BJ)/ECP/def2-TZVP level using a quasi-relativistic small-core pseudopotential for gold, along with atom-pairwise corrections for dispersion forces. First, we note an excellent agreement between X-ray and DFT optimized structures, with differences in Au–L bond-lengths of less than 0.02 Å, except for the Au–H bonds, where values determined by X-ray diffraction are often much larger (by up to 0.15 Å) than found computationally (cf. Figure S48 in Supporting Information). The precise detection of the hydride position by X-ray crystallography, however, suffers from weak scattering of X-rays by light H atoms and these data should be taken with caution. The reliability of DFT-determined Au–H bond-lengths is demonstrated by the excellent agreement between computed and experimental ¹H hydride shifts for the optimized structures, with a standard deviation of 0.4 ppm (see Figure S50 in Supporting Information). We also note a very good match between experimental and calculated ²J_{H,P} coupling constants in the hydrido phosphine complexes **9** (²J_{expt} = 32.6 Hz; ²J_{calcd} = 31.4 Hz) and **10** (²J_{expt} = 32.3 Hz; ²J_{calcd} = 30.9 Hz).

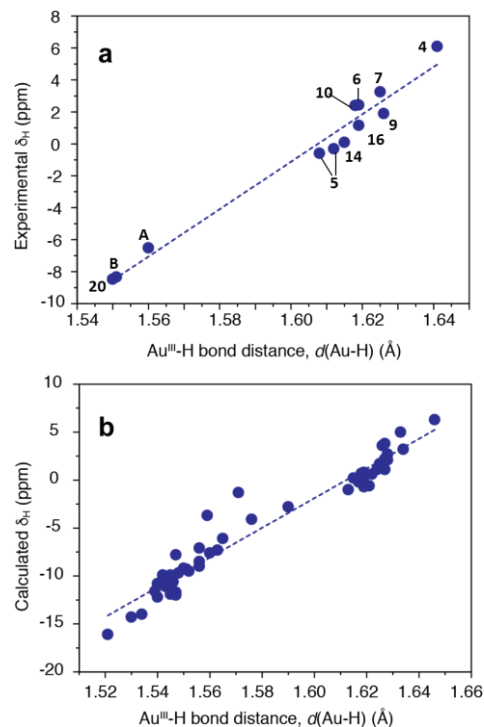
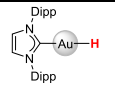
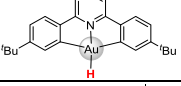
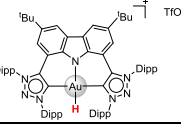
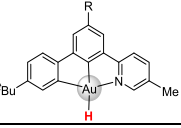
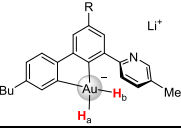
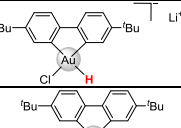
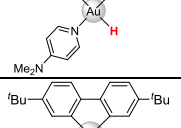
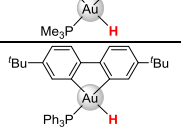
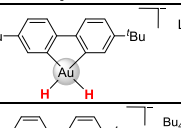
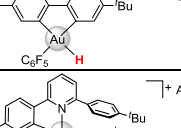
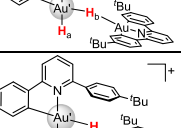
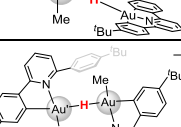
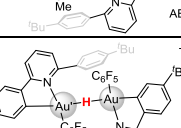
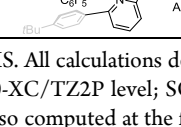
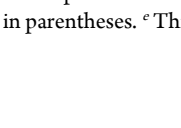


Figure 3. Dependence of experimental (a) and computed (b) ¹H NMR chemical shifts of terminal Au–H hydride atoms (in ppm vs. TMS) on the Au–H bond-length (Å) for gold(III) complexes with diverse ligand environments. The Au–H bond distances were obtained computationally at the DFT (PBE0-D3(BJ))/def2-TZVP level. Figure 3b contains both experimentally characterized and hypothetical Au(III) hydride complexes (cf. Table 1 and Tables S2–S4 in SI for numerical data). Linear regressions: (a) $\delta_{\text{H}} = 149.67 d(\text{Au-H}) - 240.57$, $R^2 = 0.970$; (b) $\delta_{\text{H}} = 155.1 d(\text{Au-H}) - 249.97$, $R^2 = 0.950$.

Table 1. DFT optimized Au–H bond-lengths (in Å) and computed and experimental ¹H NMR hydride chemical shifts of gold hydrides ^a

Complex		$d(\text{Au-H})$ [Å]	δ_{2c} (δ_{SO}) ^b	δ_{4c} ^c	$\delta_{\text{expt.}}$ ^d
 (IPr)AuH		1.611	+3.44 (+4.73)	+3.93	+3.38 (CD ₂ Cl ₂) ⁴ +5.11 (C ₆ D ₆) ⁴
 A		1.560	-6.51 (-7.06)	-6.51	-6.51 (CD ₂ Cl ₂) ⁵
 B		1.553	-8.87 (-9.12)	-8.65	-8.34 (CD ₂ Cl ₂) ⁷
 4		1.641	+6.03 (+4.74)	+6.17	+6.09 (CD ₂ Cl ₂) ^e +6.33 (THF- <i>d</i> ₈) ^e +6.99 (C ₆ D ₆) ^e
 5	<i>H_a</i> <i>H_b</i>	1.612 1.608	-0.68 (-0.47) -1.05 (-0.94)	-0.33 -0.70	-0.31 (THF- <i>d</i> ₈) ^e -0.59 (THF- <i>d</i> ₈) ^e
 6		1.619	+1.81 (+0.34)	+2.35	+2.43 (THF- <i>d</i> ₈) ^e
 7		1.625	+3.34 (+2.97)	+3.53	+3.25 (THF- <i>d</i> ₈) ^e
 9		1.628	+1.07 (+1.23)	+1.25	+1.89 (THF- <i>d</i> ₈) ^e
 11		1.616	+2.58 (+2.69)	+2.55	+2.40 (THF- <i>d</i> ₈) ^e
 14		1.618	-0.67 (-0.52)	-0.30	+0.09 (THF- <i>d</i> ₈) ^e +1.00 (tol- <i>d</i> ₈) ^e
 16		1.619	+0.28 (-0.35)	+0.68	+1.15 (THF- <i>d</i> ₈) ^e
 20	Au'- <i>H_a</i> Au- <i>H_b</i> Au'- <i>H_b</i>	1.550 1.644 1.793	-9.33 (-9.80) -5.67 (-2.61)	-8.67 -5.00	-8.47 (CD ₂ Cl ₂) ^e -4.93 (CD ₂ Cl ₂) ^e
 21	Au'- <i>H</i> Au- <i>H</i>	1.791 1.636	-5.82 (-2.90)		-5.14 (CD ₂ Cl ₂) ^e
 22a	Au'- <i>H</i> Au- <i>H</i>	1.723 1.723	-2.47 (-1.76)		-2.53 (CD ₂ Cl ₂) ^e
 22b	Au'- <i>H</i> Au- <i>H</i>	1.761 1.761	-2.03 (-1.50)		-2.21 (CD ₂ Cl ₂) ^e

^a In ppm vs. TMS. All calculations done for PBE0-D3(BJ)/ECP/def2-TZVP optimized structures (see SI). ^b Chemical shifts computed at the 2c-ZORA(SO)/PBE0-XC/TZ2P level; SO-induced contributions to hydride shifts, δ_{SO} , are given in parentheses. ^c For comparative purposes, the hydride shifts were also computed at the four-component, fully relativistic 4c-mDKS/PBE0/Dyall-VDZ/IGLO-II level. ^d Solvents used in NMR measurements are given in parentheses. ^e This work.

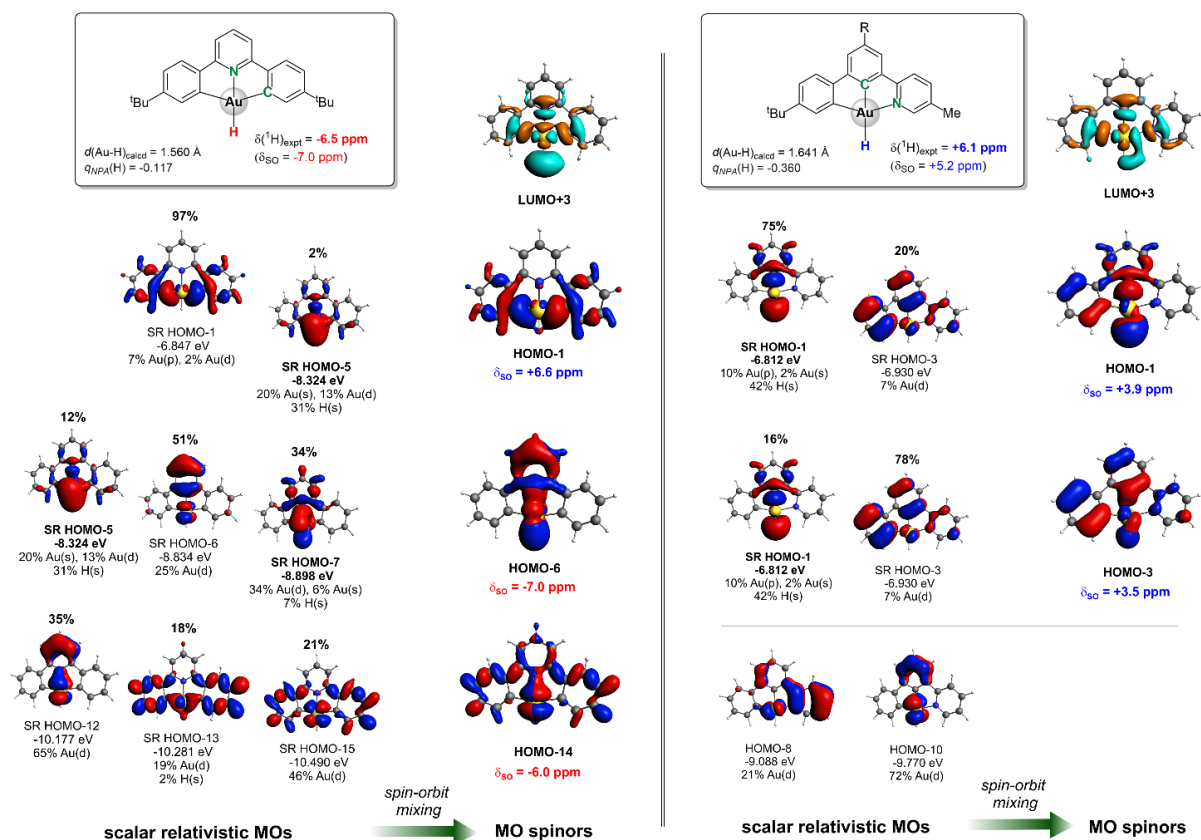


Figure 4. Relevant frontier MOs at scalar-relativistic (SR) level and their mixing to two-component spinors responsible for the overall differences in the ^1H hydride shifts of (C^NC)AuH (left) and (C^CN)AuH (right). Only one of two degenerate spinors is shown. The corresponding MOs are shown as isosurface plots (0.03 a.u.), with the hydride ligand generally being placed at the bottom. The mixing percentage of SR MOs in spinors is indicated above the corresponding SR MOs.

The experimental ^1H NMR shifts of terminal hydride atoms are found to correlate well with DFT optimized Au–H distances (Figure 3a), which suggests the potential use of ^1H NMR spectroscopy in refining precise hydride positions and explains, *inter alia*, the striking downfield ^1H shift in (C^CN)AuH (4). Interestingly, complexes in Table 1 with longer and more ionic Au–H bonds feature high-frequency (downfield) hydride shifts, which contrasts with organic C–H compounds.³³ To explore the generality of the linear $\delta(^1\text{H})$ vs. $d(\text{Au-H})$ relationship (Figure 3) and to understand the trends in light of electronic structure, a more thorough analysis of ^1H hydride shifts for a larger set of Au(III) hydrides was performed (see Table 1 and Tables S1–S4 in the SI for numeric data).

Decomposition of the computed ^1H shieldings into diamagnetic, paramagnetic and spin-orbit contributions shows that the trends in isotropic hydride shifts are dominated by the δ_{SO} term (Table 1 and Tables S1–S4 in the SI). Artificial elongation/shortening of Au–H bonds by a value of 0.05 Å from their optimized values in selected gold(III) hydrides causes only a small change in ^1H hydride shifts (< 1 ppm, data not shown), and thus the surprisingly good correlation between $\delta(^1\text{H})$ and $d(\text{Au-H})$ has an indirect rather than direct origin.^{20c} The opposite sign of the ^1H hydride shifts of the coordination isomers (C^CN)AuH and (C^NC)AuH should thus be attributed to different electronic structures (cf. Figure 4) and is rationalized below in terms of molecular orbitals contributing dominantly to δ_{SO} .

Analysis of the δ_{SO} contributions at the 2c-ZORA level show that the hydride deshielding in (C^CN)AuH, with the strong C-anionic *trans* ligand, is dominated by two spinors, HOMO-1 and HOMO-3, both composed from the $\sigma(\text{Au-H})$ -type SR HOMO-1 (with an appreciable gold 6p character) and a primarily ligand-centered π -type orbital with little metal character, SR HOMO-3 (note that both the occupied MOs are magnetically coupled mainly with an antibonding $\sigma^*(\text{Au-H})$ -type orbital, LUMO+3). Since “shielding” Au($d\pi$)-type MOs (SR HOMO-8, SR HOMO-10) lie energetically far below the $\sigma(\text{Au-H})$ MO (by more than 2 eV), these two types of scalar relativistic MOs do not mix with each other upon inclusion of SO coupling, that hinders hydride shielding and results in the high-frequency hydride shift. In contrast, the ^1H shielding for the (C^NC)AuH complex, bearing a weak *trans* N-donor ligand, is dominated by magnetic couplings between the Au($d\pi$)-type occupied and $\sigma^*(\text{Au-H})$ virtual MOs. The highest $\sigma(\text{Au-H})$ -type MO is energetically close to the Au($d\pi$) orbitals, with $\Delta E \sim 0.5$ eV, and the deshielding effect of the former diminishes upon SO mixing with Au($d\pi$)-based MOs.³⁴

As the comparison between the tethered (C^CN) and non-tethered (C^C)N ligand systems in complexes 4 and 7 shows, the steric constraint imposed by the C^CN pincer ligand also has an important effect. In C^CN the *trans*-influence of C is increased, leading to a significant lengthening of the Au–H bond

(1.641 Å in **4** vs. 1.625 Å in **7**) and a further deshielding of the hydride NMR resonance by about 3 ppm.

Theoretical papers relating ^1H NMR hydride shifts as a function of the *trans* ligand strength have appeared very recently.^{20c,21,22b} However, the influence of ligands in *cis*-position has so far not been explored. Since in square-planar complexes both *cis* and *trans* effects are operative, we performed calculations for three series: *trans*-[HAu(C₆H₅)₂L]^q, *cis*-[HAu(bph)L]^q and *cis*-[HAu(ppy)L]^{q+1} (bph = 2,2'-biphenyl dianion, ppy = 2-phenylpyridine anion; q = 0 or -1) in order to study the influences of *cis* and *trans* ligands separately for a wide range of common σ -donor and π -acceptor ligands (see SI, Tables S2-S4). The ligand effects on the ^1H hydride shifts are depicted in Figure 5.

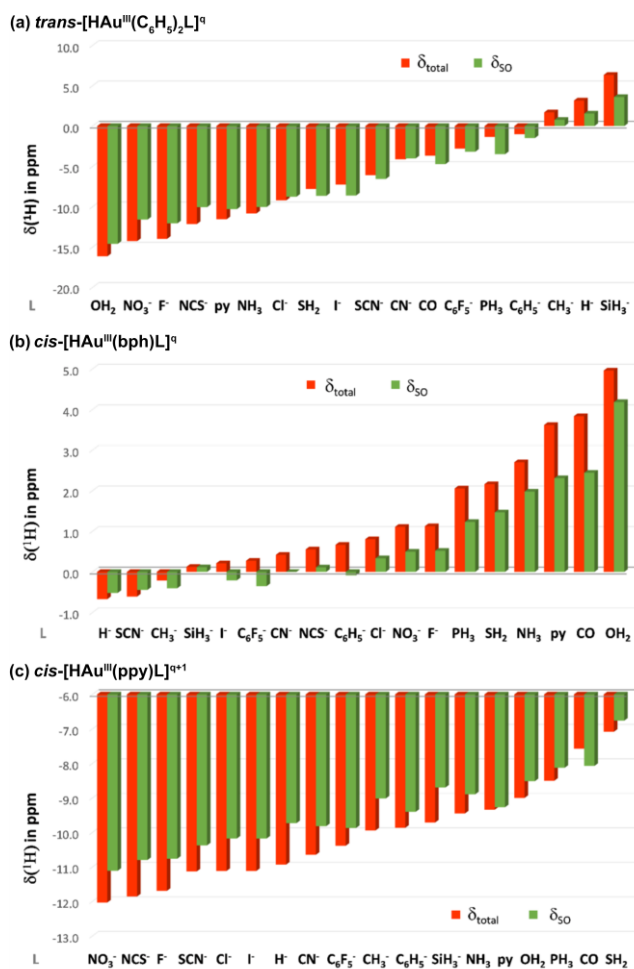


Figure 5. Dependence of the computed ^1H hydride shifts (δ_{total}) and spin-orbit-induced shift contributions (δ_{SO}) on (a) the *trans* ligand L in the *trans*-[HAu^{III}(C₆H₅)₂L]^q; (b) the *cis*-ligand in the *cis*-[HAu^{III}(bph)L]^q and (c) the *cis*-ligand in the *cis*-[HAu^{III}(ppy)L]^{q+1} series (2c-ZORA(SO)/PBE0-XC/TZ2P results; see Tables S2-S4 in SI for numerical data).

Trans-ligands produce chemical shift changes that are roughly four times larger than *cis*-ligand effects, consistent with the much larger variation in Au-H distances in the *trans* case and the strikingly different ordering and relative energies of $\sigma(\text{Au-H})$ -type and Au(d_{π}) orbitals. The influence of *trans* ligands on the ^1H shift spans about 22.5 ppm, with H₂O as the weakest donor investigated here showing the highest SO shielding contribution, and SiH₃⁻ the highest SO deshielding. Hydride shifts and Au-H bond-lengths in

gold(III) complexes follow a trend similar to the one observed for linear LAu^IH hydrides (see SI, Figure S50 and Tables S1 and S2), with the ^1H shifts in the Au(III) series being systematically shifted upfield.³⁵

Ligands in *cis*-positions have a weaker influence on hydride shifts (spanning about 6 ppm) but show the opposite trend: the weakest σ -donors (and strongest π -acceptors) exhibit the highest deshielding (the most positive ^1H hydride shifts). As demonstrated for the *cis*-[HAu(bph)L]^q series with L = NH₃, PH₃, CH₃ and SiH₃⁻ (cf. Figure 5), the *cis* ligand influence has the same qualitative explanation as postulated for the *trans*-influence above, but ligands with stronger *trans*-influence located in the *cis*-position decrease the energy gap between the highest-lying $\sigma(\text{Au-H})$ bonding MO and Au(d_{π})-based MO, just the opposite of what is seen for the *trans*-influence (see SI, Figures S51-S52).

According to the data for the *cis*-[HAu(bph)L]^q and *cis*-[HAu(ppy)L]^{q+1} series, the order of increasing *cis* ligand influence depends also on the *trans* ligand. However, in general the strongest *cis*-influence (reflected in the longest Au-H bonds and the most downfield ^1H shifts) is observed for neutral weak σ -donors (such as S, N and O-based ligands) and CO, while anionic ligands exert the weakest *cis*-influence, consistent with our experimental NMR data collected in Table 1.

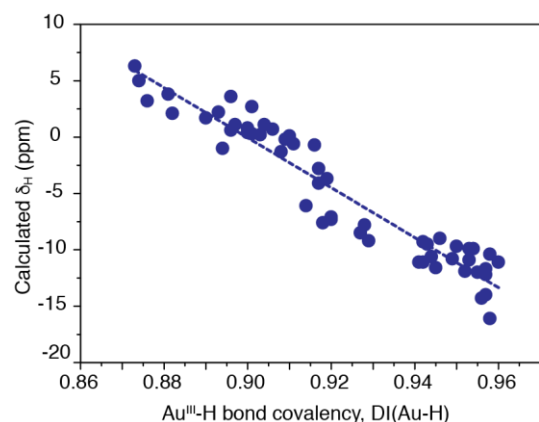


Figure 6. Correlation of computed ^1H NMR hydride shifts (in ppm vs. TMS) with QAIM delocalization indices, DI(Au-H), as a measure of the bond covalency, for a series of mononuclear Au(III) hydride complexes (cf. SI, Tables S2-S4 for numerical data).

To conclude, the observed correlation between measured ^1H hydrides shifts and Au-H bond-lengths has an indirect origin, but works surprisingly well for a wider set of studied mononuclear Au(III) hydrides (Figure 3). This can be attributed to decisive SO-shift contribution and only marginal changes in paramagnetic shielding. Since Au-H distances correlate roughly with QAIM delocalization indices of the Au-H bond, a reasonable relationship is also established between ^1H NMR hydrides shifts and Au-H bond covalency (see Figure 6): the more ionic the Au-H bond, the more positive is the hydride shift.^{36,37} Note that the differences in Au-H bond covalency could also explain the similar reactivities of gold(III) hydrides with C-anionic *trans* ligands (with δ_{H} ranging from -0.6 to +7.0 ppm) and of gold(I) hydride (IPr)AuH (δ_{H} = 3.38 ppm/CD₂Cl₂) towards alkynes: both these compound types insert DMAD but not less activated alkynes, whereas the gold(III)

pincer hydride ($C^{\wedge}N^{\wedge}C$)AuH ($\delta_H = -6.51$ ppm/ CD_2Cl_2) with a much shorter and more covalent Au–H bond behaves differently and adopts a different mechanism.

CONCLUSIONS

In summary, this work shows that a rather diverse range of gold(III) hydride complex types is accessible using $C^{\wedge}C$ chelate ligands, and that stabilization by tridentate pincer ligands is neither a requirement nor a guarantee for thermal stability. Suitable combinations of *cis* and *trans* donors provide access to the first examples of stable Au(III) hydrido phosphine complexes, as well as to anionic hydrido halide, hydrido aryl, and even dihydrido complexes. The biphenyl-based $C^{\wedge}C$ chelate imparts a remarkable stability towards reductive elimination and successfully suppresses H–C and even H–H coupling. $C^{\wedge}N$ chelate complexes derived from proto-deauration of ($C^{\wedge}N^{\wedge}C$) pincer precursors proved to be a convenient platform for intercepting the first examples of bridging gold(III) hydrides. The chemistry of the new $C^{\wedge}C$ - and $C^{\wedge}C^{\wedge}N$ -based gold hydrides, with strong C-donors *trans* to H, was found to differ significantly from that of the $C^{\wedge}N^{\wedge}C$ (weak *trans* donor) coordination isomers; e.g. the former react only with DMAD but not less activated alkyl or aryl acetylenes, while for the latter the opposite is found. Chemical reactivity correlates with the hydride 1H NMR chemical shift, since both are subject to *trans* and *cis* ligand effects. Based on detailed quantum-chemical calculations and analysis including relativistic spin-orbit coupling effects, a linear relationship could be established between the computed Au–H bond distances, the hydridic character of the Au–H bond, and the hydride NMR chemical shifts. Strong *trans* effect ligands, such as C^- in ($C^{\wedge}C^{\wedge}N$)AuH, raise the deshielding σ (Au–H) orbital and increase the energetic separation from orbitals with shielding Au(d_{π})-type MO, resulting in deshielding (positive chemical shift), whereas in ($C^{\wedge}N^{\wedge}C$)AuH σ (Au–H) and Au(d_{π}) are close in energy, so that the hydride shift is dominated by the shielding SO contribution. Whereas *trans*-ligand influence calculated for a sequence of hypothetical complexes cover a range of over 22 ppm, *cis*-ligand influence is more limited, about 6 ppm, although both these effects are mutually interdependent. The effect of *cis*-ligands follows an approximate inverse order to *trans*-ligands, with the strongest *cis*-influence (and the longest Au–H bonds) being observed for the weakest neutral σ -donors. This appears to be the first systematic evaluation of *cis*-ligand effects on 1H chemical shifts in square-planar d^8 systems.

EXPERIMENTAL SECTION

General Considerations. When required, manipulations were performed using standard Schlenk techniques under dry argon or using a nitrogen-filled MBraun Unilab glovebox equipped with a high capacity recirculator (<1.0 ppm O_2 and H_2O). Argon was purified by passing through columns of supported P_2O_5 with moisture indicator and of activated 4 Å molecular sieves. Anhydrous solvents were freshly distilled from the appropriate drying agents and degassed. Triphenylphosphine (99%), tris(*p*-tolyl)phosphine (98%), trimethylphosphine (1.0M in THF), dimethylaminopyridine (DMAP, >99%), lithium triethylborohydride (1.0 M in THF), dimethyl acetylenedicarboxylate (DMAD, 99%) trimethoxysilane (95%), were obtained by Sigma Aldrich and dried, when necessary. Solid $LiAlH_4$ was obtained by vacuum-drying a commercial solution in THF (Sigma Aldrich). CD_2Cl_2 (Apollo Scientific), THF– d_8

and toluene– d_8 (Fluorochem Ltd.) were freeze-pump-thaw degassed over CaH_2 , distilled and stored over activated 4 Å molecular sieves. $C_6F_5Ag(CH_3CN)$,³⁸ $[(C^{\wedge}C)AuCl]_2$,¹⁶ $(C^{\wedge}C)AuCl(py)$ (2),¹⁶ $(C^{\wedge}N^{\wedge}C)AuH$,⁵ $(C^{\wedge}N^{\wedge}C)AuMe$,³⁹ $(C^{\wedge}N^{\wedge}C)AuC_6F_5$,⁴⁰ $[H(OEt)_2][H_2N\{B(C_6F_5)_3\}_2]$ ²⁸ (HAB_2) were synthesized according to literature procedures. Proto-deaured species $[(C^{\wedge}N-CH)AuMe][AB_2]$ (**3a**) and $[(C^{\wedge}N-CH)AuC_6F_5][AB_2]$ (**3b**) were generated within the glovebox, as reported previously.¹⁷

Low-temperature *in situ* NMR experiments were performed under anhydrous and anaerobic conditions by using screw cap NMR tubes equipped with a PTFE septum. In a typical experiment, the gold precursor was loaded into the NMR tube inside a glovebox and dissolved in the appropriate solvent. Successively, the sample was inserted into a cold bath at 195 K and the desired reagents were injected through the septum by using a micrometric gas-tight syringe. The cold sample was then inserted into the pre-cooled NMR probe and characterized. 1H , 1H PGSE, 1H inversion recovery, ^{19}F , $^{13}C\{^1H\}$, 1H COSY, 1H NOESY, 1H , ^{13}C HMQC, and 1H , ^{13}C HMB NMR experiments were recorded on a Bruker DPX-300 spectrometer equipped with a 1H , BB smartprobe and Z-gradients. 1H NMR spectra were referenced to the residual protons of the deuterated solvent. ^{13}C NMR spectra were referenced to the D-coupled ^{13}C signals of the solvent. ^{19}F NMR spectra were referenced to an external standard of $CFCl_3$. ^{31}P NMR spectra were referenced to an external standard of H_3PO_4 85%. Photoisomerization experiments were performed by using a Blak-Ray B-100 Series high-powered UV lamp and by irradiating solutions contained in J-Young NMR tubes.

Synthesis and characterization of new gold precursors

($C^{\wedge}C^{\wedge}N$)AuCl (1). This complex was synthesized in 89% yield by following literature procedures,¹⁵ using 2-bromo-5-methyl pyridine as ligand precursor. 1H NMR (300.13 MHz, CD_2Cl_2 , 297K, J values in Hz): δ 8.78 (brs, 1H, H1), 7.80 (d, $^4J_{HH} = 1.6$, H16), 7.72 (AB system, 2H, H3+H4), 7.61 (d, $^3J_{HH} = 8.4$, 2H, H19), 7.52 (d, $^3J_{HH} = 8.4$, 2H, H20), 7.39 (d, $^4J_{HH} = 1.5$, H7), 7.34 (d, $^4J_{HH} = 1.5$, H9), 7.23 (AB system, 2H, H13+H14), 2.33 (s, 3H, Me), 1.38 (s, 9H, C(21)CMe₃), 1.32 ppm (s, 9H, C(15)CMe₃). $^{13}C\{^1H\}$ NMR (75.47 MHz, CD_2Cl_2 , 297 K): δ 164.7 (s, C11), 160.1 (s, C5), 151.0 (s, C15), 150.8 (s, C21+C12), 150.4 (s, C17), 149.4 (s, C10), 148.7 (s, C1), 141.2 (s, C3+C6), 140.0 (s, C8), 137.9 (s, C18), 135.2 (s, C2), 131.4 (s, C16), 126.9 (s, C19), 125.8 (s, C20), 124.4 (s, C14), 121.5 (s+s, C13+C9), 120.2 (s, C7), 119.8 (s, C4), 35.0 (s, C(15)CMe₃), 34.5 (s, C(21)CMe₃), 31.1 (s, C(15)CMe₃ or C(21)CMe₃) 31.0 (s, C(21)CMe₃ or C(15)CMe₃), 18.2 ppm (s, Me). Calcd for $C_{32}H_{33}AuNCl$ (found): C, 57.86 (57.69); H, 5.01 (4.94); N, 2.11 (2.18) %.

($C^{\wedge}C$)AuCl(Ptol₃). $[(C^{\wedge}C)AuCl]_2$ (200 mg, 0.2 mmol) was stirred in dichloromethane (30 ml) with excess tris-*para*-tolylphosphine (120 mg, 0.4 mmol) until a clear solution was obtained. The reaction mixture was filtered through celite and the solvent removed under reduced pressure. Hexane was added, the mixture sonicated briefly and the white solid powder filtered and washed with hexane. It was then recrystallized from Et_2O /hexane to afford $(C^{\wedge}C)AuCl(Ptol_3)$ (290 mg, 90%). 1H NMR (300.13 MHz, CD_2Cl_2 , 297K, J values in Hz): δ 8.38 (dd, $^4J_{HP} = 9.5$, $^4J_{HH} = 1.8$, 1H, H2), 7.53–7.59 (m, 6H, *o*-tol₃), 7.24–7.32 (m, 8H, *m*-tol₃+H5+H5'), 7.19 (dd, $^3J_{HH} = 8.0$ $^4J_{HH} = 1.6$, 1H, H4), 7.03 (dd, $^3J_{HH} = 8.0$ $^4J_{HH} = 1.8$, 1H, H4'), 6.92 (dd, $^4J_{HP} = 3.4$, $^4J_{HH} = 1.8$, 1H, H2'), 2.39 (s, 9H, Me), 1.31 (s, 9H, CMe₃), 0.67 ppm (s, 9H,

CMe_3). $^{31}\text{P}\{^1\text{H}\}$ NMR (121.49 MHz, CD_2Cl_2 , 297 K): 40.2 ppm. $^{13}\text{C}\{^1\text{H}\}$ NMR (75.47 MHz, CD_2Cl_2 , 297 K, J values in Hz): δ 166.1 (d, $^2J_{\text{CP}} = 129.6$, C1), 154.0 (d, $^2J_{\text{CP}} = 7.3$, C1'), 151.3 (d, $^3J_{\text{CP}} = 4.5$, C6'), 149.7-149.6 (m, C6+C3), 149.2 (d, $^4J_{\text{CP}} = 2.7$, C3), 142.3 (d, $^4J_{\text{CP}} = 2.4$, CMe tols), 135.1 (d, $^2J_{\text{CP}} = 11.5$, α -tols), 134.2 (d, $^3J_{\text{CP}} = 10.2$, C2'), 130.5 (d, $^3J_{\text{CP}} = 1.8$, C2), 129.4 (d, $^4J_{\text{CP}} = 11.2$, m -tols), 125.1 (d, $^1J_{\text{CP}} = 51.0$, *ipso*-C tols), 124.5 (br s, C4), 123.8 (s, C4'), 120.7 (s, C5'), 120.4 (d, $^4J_{\text{CP}} = 7.6$, C5), 35.3 (s, CMe_3), 35.4 (s, CMe_3 '), 31.2 (s, CMe_3), 30.4 (s, CMe_3 '), 21.2 ppm (s, Me tols). Calcd for $\text{C}_{41}\text{H}_{45}\text{AuClIP}$ (found): C, 61.44 (61.36); H, 5.66 (5.67) %

($\text{C}^{\wedge}\text{C}$)AuCl(PMe_3). [$(\text{C}^{\wedge}\text{C})\text{AuCl}$] $_2$ (270 mg, 0.27 mmol) was stirred in THF (10 ml) under Ar. Excess trimethylphosphine (0.5 ml of 1M solution in THF, 0.5 mmol) was added at 25 °C and the mixture was stirred until a clear solution was obtained. The reaction mixture was filtered through celite and the solvent removed under reduced pressure. Hexane was added, the mixture sonicated briefly and the white solid powder filtered and washed with hexane to afford ($\text{C}^{\wedge}\text{C}$)AuCl(PMe_3) (250 mg, 81%). ^1H NMR (300.13 MHz, CD_2Cl_2 , 297K, J values in Hz): δ 8.29 (br d, 1H, H2), 7.43-7.13 (br m, 5H, H4+H4'+H5+H5'+H2'), 1.85 (d, $^2J_{\text{HP}} = 10.8$, PMe_3), 1.34 ppm (s, 18H, $\text{CMe}_3+\text{CMe}_3$ '). $^{31}\text{P}\{^1\text{H}\}$ NMR (121.49 MHz, CD_2Cl_2 , 297 K): 3.4 ppm. $^{13}\text{C}\{^1\text{H}\}$ NMR (75.47 MHz, CD_2Cl_2 , 297 K, J values in Hz): δ 165.2 (d, $^2J_{\text{CP}} = 138.4$, C1), 153.2 (br s, C1'), 151.6 (s, C6'), 149.6 (m, C3+C3'), 149.2 (s, C6), 130.0 (s, C2+C2'), 124.6 (s, C4 or C4'), 124.4 (s, C4' or C4), 121.5 (s, C5'), 120.4 (brd, $^5J_{\text{CP}} = 6.6$, C5), 35.2 (s, CMe_3 or CMe_3 '), 31.2 (s+s, $\text{CMe}_3+\text{CMe}_3$ '), 14.2 ppm (d, $^1J_{\text{CP}} = 30.4$, PMe_3). Calcd for $\text{C}_{23}\text{H}_{33}\text{AuClP}$ (found): C, 48.22 (48.43); H, 5.81 (5.89) %.

($\text{C}^{\wedge}\text{C}$)Au(C_6F_5)(py). $\text{C}_6\text{F}_5\text{Ag}(\text{CH}_3\text{CN})$ (93 mg, 0.3 mmol) in Et_2O (5 ml) was added to a solution of **2** (170 mg, 0.3 mmol) in dichloromethane (5 mL) in a centrifuge tube, with immediate formation of AgCl. After 5 min, the tube was centrifuged. The clear solution was decanted and the solvent removed under reduced pressure to afford the product as a white solid (144 mg, 60 %). ^1H NMR (300.13 MHz, CD_2Cl_2 , 297K, J values in Hz): δ 8.78 (d, $^3J_{\text{HH}} = 5.2$, 2H, α -py), 8.04 (t, $^3J_{\text{HH}} = 7.8$, 1H, p -py), 7.68 (t, $^3J_{\text{HH}} = 6.7$, 2H, m -py), 7.37 (d, $^3J_{\text{HH}} = 8.0$, 1H, H5), 7.32 (d, $^3J_{\text{HH}} = 8.0$, 1H, H5'), 7.18-7.22 (m, 2H, H4+H4'), 6.84 (d, $^4J_{\text{HH}} = 1.2$, 1H, H2), 6.34 (d, $^4J_{\text{HH}} = 1.2$, 1H, H2'), 1.50 (s, 9H, CMe_3), 1.08 ppm (s, 9H, CMe_3 '). ^{19}F NMR (282 MHz, CD_2Cl_2 , 297K): δ -120.8 (m, α -F), -159.6 (t, p -F), -161.9 (m, m -F) ppm. $^{13}\text{C}\{^1\text{H}\}$ NMR (75.47 MHz, CD_2Cl_2 , 297 K): δ 151.5 (s, C1'), 150.1 (s, α -py), 149.9 (s, C1), 149.5 (s, C6+C6'), 144.5 (s, C3+C3'), 140.1 (s, p -py), 132.4 (s, C2), 127.7 (s, C2'), 127.1 (s, m -py), 124.5 (s, C5), 124.1 (s, C5'), 121.1 (s, C4'), 120.3 (s, C4), 34.6 (s, CMe_3), 34.4 (s, CMe_3 '), 30.92 (s, CMe_3), 30.89 ppm (s, CMe_3 '). Calcd for $\text{C}_{31}\text{H}_{29}\text{AuF}_5\text{N}$ (found): C, 52.6 (51.96); H, 4.13 (4.55); N, 1.98 (2.01) %.

[Bu_4N^+][($\text{C}^{\wedge}\text{C}$)AuCl(C_6F_5)] (15**)**. ($\text{C}^{\wedge}\text{C}$)Au(C_6F_5)(py) (50 mg, 71 μmol) was stirred in dichloromethane (5 mL) in the presence of excess tetrabutylammonium chloride (30 mg, 0.1 mmol) for 1 h. The solvent was removed under reduced pressure. Dichloromethane (5 mL) was added and the mix stirred again for 1 h. The solvent was removed under reduced pressure. The residue was sonicated in Et_2O and the white powder filtered to yield **15** (45 mg, 98 %). ^1H NMR (300.13 MHz, CD_2Cl_2 , 297K, J values in Hz): δ 8.24 (d, $^4J_{\text{HH}} = 2.0$, 1H, H2), 7.25 (d, $^3J_{\text{HH}} = 8.0$, 1H, H5), 7.24 (d, $^3J_{\text{HH}} = 8.0$, 1H, H5'), 7.12 (dd, $^3J_{\text{HH}} = 8.0$, $^4J_{\text{HH}} = 1.9$, 1H, H4), 7.08 (dd, $^3J_{\text{HH}} = 8.0$, $^4J_{\text{HH}} = 1.9$, 1H, H4'), 6.81 (d, $^4J_{\text{HH}} = 1.6$, 1H, H2'),

2.99-3.06 (m, 8H, $\text{CH}_3(\text{CH}_2)_2\text{CH}_2\text{N}$), 1.41-1.52 (m, 8H, $\text{CH}_3\text{CH}_2\text{CH}_2\text{CH}_2\text{N}$), 1.33 (s, 9H, CMe_3), 1.26-1.32 (m, 8H, $\text{CH}_3\text{CH}_2(\text{CH}_2)_2\text{N}$), 1.10 (s, 9H, CMe_3 '), 0.92 ppm (t, $^3J_{\text{HH}} = 7.6$, 12H, $\text{CH}_3(\text{CH}_2)_3\text{N}$). ^{19}F NMR (282 MHz, CD_2Cl_2 , 297K): -119.6 (m, α -F), -162.3 (t, p -F), -163.2 (m, m -F) ppm. $^{13}\text{C}\{^1\text{H}\}$ NMR (75.47 MHz, CD_2Cl_2 , 297 K): δ 151.1 (s, C2'), 150.2 (s, C2), 149.2 (s, C5'), 148.7 (s, C5), 131.3 (s, C4'), 130.0 (s, C4), 129.9 (s, C1'), 123.4 (s, C3'), 123.1 (s, C3), 120.3 (s, C6'), 120.1 (s, C1), 119.5 (s, C6), 58.6 (s, $\text{CH}_3(\text{CH}_2)_2\text{CH}_2\text{N}$), 35.0 (s, CMe_3 '), 34.3 (s, CMe_3), 31.4 (s, C8'), 30.9 (s, C8), 23.8 (s, $\text{CH}_3\text{CH}_2\text{CH}_2\text{CH}_2\text{N}$), 19.6 (s, $\text{CH}_3\text{CH}_2(\text{CH}_2)_2\text{N}$), 13.4 ppm (s, $\text{CH}_3(\text{CH}_2)_3\text{N}$). Calcd for $\text{C}_{42}\text{H}_{60}\text{AuClF}_5\text{N}$ (found): C, 55.64 (55.64); H, 6.68 (6.58); N, 1.55 (1.68) %.

In situ NMR experiments and data

($\text{C}^{\wedge}\text{C}^{\wedge}\text{N}$)AuH (4**)**. ($\text{C}^{\wedge}\text{C}^{\wedge}\text{N}$)AuCl (**1**) (15 mg, 0.0226 mmol) was loaded into a screw cap NMR within the glovebox and approximately 0.7 mL of dry THF- d_6 were added under Ar. The resultant suspension was sonicated at room temperature for 10 s to obtain a pale-yellow solution. The NMR tube was then inserted in a cold bath at 195K and, using a microsyringe, LiHBEt_3 (1 equiv, 22.6 μL of a 1.0 M solution in THF) was injected through the septum. The sample was quickly shaken to obtain a bright yellow solution and inserted into the NMR probe and analyzed at 253K. ^1H NMR (300.13 MHz, THF- d_6 , 253 K, J values in Hz): δ 8.86 (s, 1H, H1), 8.00 (d, 1H, $^3J_{\text{HH}} = 8.3$, H4), 7.89 (d, 1H, $^3J_{\text{HH}} = 8.3$, H3), 7.70 (s, 2H, H7+H16), 7.65 (d, 2H, $^3J_{\text{HH}} = 8.3$, H19), 7.58 (s, 1H, H9), 7.50 (d, 2H, $^3J_{\text{HH}} = 8.3$, H20), 7.37 (d, 1H, $^3J_{\text{HH}} = 8.1$, H13), 7.17 (dd, 1H, $^3J_{\text{HH}} = 8.1$, $^4J_{\text{HH}} = 1.8$, H14), 6.33 (s, 1H, Au-H), 2.36 (s, 3H, Me), 1.38 (s, 9H, C(21) CMe_3), 1.34 ppm (s, 9H, C(15) CMe_3). $^{13}\text{C}\{^1\text{H}\}$ NMR (75.47 MHz, THF- d_6 , 253 K): δ 184.2 (s, C11), 165.9 (s, C5), 156.0 (s, C1), 154.9 (s, C12), 151.8 (s, C10), 150.8 (s, C15), 150.2 (s, C21), 145.3 (s, C17), 144.3 (s, C6), 141.5 (s, C3), 140.8 (s, C8), 139.9 (s, C18), 138.4 (s, C16), 136.3 (s, C2), 127.4 (s, C19), 126.1 (s, C20), 123.8 (s, C14), 121.9 (s, C13), 120.9 (s, C7+C9), 120.8 (s, C4), 35.1 (s, C(15) CMe_3), 35.0 (s, C(21) CMe_3), 31.5 (s+s, C(15) CMe_3 +C(21) CMe_3), 17.9 ppm (s, Me). T₁ (253 K, THF- d_6): Au-H 1.30 s.

Li[($\text{C}^{\wedge}\text{C}^{\wedge}\text{N}$)AuH $_2$] (5**)**. *Procedure (a)*: In the glove box under N_2 , **1** (10 mg, 0.015 mmol) was loaded into a screw-cap NMR tube, and approximately 0.7 mL of dry THF- d_6 were added. The resultant suspension was sonicated at room temperature for 10 s to obtain a pale-yellow solution. The NMR tube was then inserted in a cold bath at 195 K and 2.0 equiv LiHBEt_3 (30.2 μL of a 1.0 M solution in THF) were injected through the septum by using a microsyringe. The sample was quickly shaken to give a colorless solution and analyzed at 263K. *Procedure (b)*: In the glovebox under N_2 , 15 mg of **1** and 3.0 equivalents of solid LiAlH_4 (2.5 mg) were loaded into a screw cap NMR tube. The NMR tube was inserted in a cold bath at 195 K and approximately 0.7 mL of dry THF- d_6 were added. The resultant dark suspension was shaken and the NMR tube was inserted into the pre-cooled NMR probe and analyzed at 203 K. ^1H NMR (300.13 MHz, THF- d_6 , 263 K, J values in Hz): δ 8.26 (s, 1H, H1), 8.08 (m, 1H, H16), 7.72 (s, 1H, H9), 7.58 (m, 4H, H3+H4+H19), 7.43 (m, 4H, H7+H13+H20), 6.98 (dd, $^3J_{\text{HH}} = 8.1$, $^4J_{\text{HH}} = 2.1$, 1H, H14), 2.37 (s, 3H, Me), 1.35 (s, 9H, (C21) CMe_3), 1.31 (s, 9H, (C15) CMe_3), -0.31 (ps t, 1H, $^2J_{\text{HH}} = 4.3$, Au-H_b), -0.59 ppm (d, 1H, $^2J_{\text{HH}} = 4.3$, Au-H_a). $^{13}\text{C}\{^1\text{H}\}$ NMR (75.47 MHz, THF- d_6 , 263 K): δ 172.3 (s, C17), 171.1 (s, C11), 167.2 (s, C5), 161.1 (s, C10), 155.4 (s, C12), 149.6 (s, C21), 149.2 (s, C6), 148.8

(s, C15), 147.5 (s, C1), 140.7 (s, C18), 140.4 (s, C16), 138.1 (s, C8), 137.0 (s, C3), 130.7 (s, C2), 126.9 (s, C19), 126.8 (s, C4), 125.9 (s, C20), 124.3 (s, C7), 120.7 (s, C14), 120.4 (s, C13), 118.6 (s, C9), 34.8 (s, C(15)CMe₃), 34.7 (s, C(21)CMe₃), 32.0 (s, C(15)CMe₃), 31.6 (s, C(21)CMe₃), 18.4 ppm (s, Me). T₁ (-20°C, THF-*d*₆): Au-H_a 0.80 s, Au-H_b 0.82 s.

Li[(C[∧]C)Au(H)Cl] (6). In a glovebox under N₂, **2** (15 mg, 0.026 mmol) was loaded into a screw-cap NMR tube and dissolved in approximately 0.7 mL of dry THF-*d*₆. The NMR tube was then inserted in a cold bath at 195 K and 2.0 equiv LiHBET₃ (52.0 μL of a 1.0 M solution in THF) were injected through the septum, using a microsyringe. The sample was quickly shaken to obtain a bright yellow solution and inserted into the NMR probe and analyzed at 213 K. ¹H NMR (300.13 MHz, THF-*d*₆, 213 K, *J* values in Hz): δ 8.01 (m, 1H, H2'), 7.72 (overlapped with py signals, 1H, H2), 7.20 (d, 1H, ³J_{HH} = 8.2, H5), 7.17 (d, 1H, ³J_{HH} = 8.2, H5'), 6.96 (br d, 1H, ³J_{HH} = 8.2, H4), 6.90 (dd, 1H, ³J_{HH} = 8.2, ⁴J_{HH} = 1.8, H4'), 2.43 (br s, 1H, Au-H), 1.27 (s, 9H, CMe₃), 1.25 ppm (s, 9H, CMe₃'). ¹³C{¹H} NMR (75.47 MHz, THF-*d*₆, 213 K): δ 174.8 (s, C1'), 153.0 (s, C6), 151.4 (s, C6'), 149.3 (s, C3), 148.4 (s, C1), 147.1 (s, C3'), 139.1 (s, C2), 129.9 (s, C2'), 121.9 (s, C4), 121.8 (s, C4'), 120.1 (s, C5), 118.9 (s, C5'), 34.7 (s, CMe₃), 34.1 ppm (s, CMe₃'), 31.2+31.1 (s+s, CMe₃+CMe₃').

(C[∧]C)AuH(DMAP) (7). A sample of **6** was generated as described above from 15 mg of **2** and kept at 195 K. Successively, 4.0 equivalents of DMAP (12.7 mg) were dissolved in 0.3 ml of dry THF-*d*₆ and injected through the septum by using a gas-tight syringe to obtain a yellow solution. The sample was then transferred into the pre-cooled NMR probe and analyzed at 253 K. ¹H NMR (300.13 MHz, THF-*d*₆, 253 K, *J* values in Hz): δ 8.32 (d, ³J_{HH} = 7.1, 2H, H7), 7.74 (ps t, ⁴J_{HH} = 2.0, 1H, H2), 7.27 (m, overlapped with py signals, H5+H5'), 7.03 (dd, ³J_{HH} = 8.1, ⁴J_{HH} = 2.0, 1H, H4), 6.99 (dd, ³J_{HH} = 8.1, ⁴J_{HH} = 2.0, 1H, H4'), 6.92 (dd, ⁴J_{HH} = 4.5, ⁴J_{HH} = 2.0, 1H, H2'), 6.89 (d, ³J_{HH} = 7.1, 2H, H8), 3.25 (brs, 1H, Au-H), 3.13 (s, 6H, NMe₂), 1.29 (s, 9H, CMe₃), 1.17 ppm (s, 9H, CMe₃'). ¹³C{¹H} NMR (75.47 MHz, THF-*d*₆, 253 K): δ 174.6 (s, C1'), 155.3 (s, C9), 153.3 (s, C6), 151.8 (s, C6'), 151.1 (s, C7), 148.8 (s, C3), 148.1 (s, C3'), 144.1 (s, C1), 139.9 (s, C2), 129.0 (s, C2'), 122.8 (s+s, C4+C4'), 119.9 (s, C5 or C5'), 119.2 (s, C5' or C5), 108.5 (s, C8), 39.0 (s, NMe₂), 35.1 (s, CMe₃'), 34.7 (s, CMe₃), 31.8 ppm (s, CMe₃+CMe₃').

(C[∧]C)AuH(PMe₃) (9). *Procedure (a):* A sample of **6** was generated as described above from 15 mg of **2** and kept at 195 K. Successively, 1.0 equivalent of PMe₃ (26 μL of a 1.0 M solution in THF) was injected through the septum by using a gas-tight syringe to obtain a pale-yellow solution. The sample was then transferred into the pre-cooled NMR probe and analyzed at 253 K. *Procedure (b):* In the glovebox, 20 mg of (C[∧]C)AuCl(PMe₃) were loaded into a screw-cap NMR tube and dissolved in approximately 0.7 mL of toluene-*d*₈. Outside the glovebox, 1.0 equiv LiHBET₃ (35 μL of a 1.0 M solution in THF) were injected through the septum by a microsyringe at room temperature to give a pale-yellow solution and a white precipitate. The solution was filtered over celite into a J Young NMR tube and dried under vacuum to afford a pale-yellow powder, which was re-dissolved in dry toluene-*d*₈ and analyzed at room temperature. ¹H NMR (300.13 MHz, THF-*d*₆, 253 K, *J* values in Hz): δ 7.94 (dt, ⁴J_{HP} = 10.0, ⁴J_{HH} = 1.7, 1H, H2), 7.58 (m, 1H, H2'), 7.32 (d, ³J_{HH} = 8.2, 1H, H5'), 7.28 (dd, ³J_{HH} = 8.2, ⁵J_{HP} = 4.1, 1H, H5), 7.06 (dd, partially overlapped with H4, 1H, H4'), 7.04

(dd, partially overlapped with H4', 1H, H4), 1.89 (d, ²J_{HP} = 10.8, 9H, PMe₃), 1.53 (brd, ²J_{HP} = 32.6, 1H, Au-H), 1.31 (s, 9H, CMe₃'), 1.28 ppm (s, 9H, CMe₃). ¹³C{¹H} NMR (75.47 MHz, THF-*d*₆, 253 K, *J* values in Hz): δ 168.4 (d, ²J_{FC} = 4.6, C1'), 160.6 (d, ²J_{FC} = 136.2, C1), 154.8 (d, ³J_{FC} = 5.5, C6), 154.1 (s, C6'), 149.3 (d, ⁴J_{FC} = 10.0, C3), 148.4 (s, C3'), 140.8 (d, ³J_{FC} = 5.4, C2), 133.0 (d, ³J_{FC} = 6.6, C2'), 123.0 (s+s, C4+C4'), 120.5 (m, H5+H5'), 35.0 (s, CMe₃'), 34.8 (s, CMe₃), 31.7 (s+s, CMe₃+CMe₃'), 15.9 ppm (d, ¹J_{CP} = 32.5, PMe₃). ³¹P{¹H} NMR (121.49 MHz, THF-*d*₆, 253 K): -8.2 ppm (s, PMe₃). ¹H NMR (300.13 MHz, Toluene-*d*₈, 298K, *J* values in Hz): δ 8.49 (dt, ⁴J_{HP} = 10.6, ⁴J_{HH} = 2.0, 1H, H2), 7.58 (d, ³J_{HH} = 8.2, 1H, H5'), 7.54 (m, 2H, H2'+H5), 7.22 (m, 2H, H4+H4'), 1.86 (dm, ²J_{HP} = 34.7, 1H, Au-H), 1.39 (s+s, 18H, CMe₃+CMe₃'), 1.03 ppm (d, ²J_{HP} = 10.2, 9H, PMe₃).

(C[∧]C)AuH(Ptol₃) (10). This complex was prepared by following the procedures described for **9**. Procedure (a) was followed by using 15 mg of **2** and 7.9 mg of P(*p*-tol)₃ (dissolved in 0.2 ml of THF-*d*₆). Procedure (b) was followed by using 15 mg of (C[∧]C)AuCl(Ptol₃) and 19 μL of a 1M LiHBET₃ solution in THF. ¹H NMR (300.13 MHz, THF-*d*₆, 213 K, *J* values in Hz): δ 8.00 (br d, ⁴J_{HP} = 9.3, H2), 7.49 (m, 6H, H8), 7.34 (m, 8H, H5+H5'+H9), 7.08 (dd, ³J_{HH} = 8.1, ⁴J_{HH} = 8.1, 1H, H4), 6.97 (m, 1H, H2'), 6.90 (dd, ³J_{HH} = 8.1, ⁴J_{HH} = 8.1, 1H, H4'), 2.38 (s, 9H, Me), 2.33 (brd, ²J_{PH} = 33.0, Au-H), 1.28 (s, 9H, CMe₃), 0.77 (s, 9H, CMe₃'). ¹³C{¹H} NMR (75.47 MHz, THF-*d*₆, 213 K, *J* values in Hz): δ 168.4 (d, ²J_{FC} = 4.7, C1'), 159.8 (d, ²J_{FC} = 129.0, C1), 153.7 (d, ³J_{FC} = 5.0, C6), 153.3 (s, C6'), 148.8 (d, ⁴J_{FC} = 9.0, C3), 147.7 (s, C3'), 142.1 (s, C10). 140.3 (d, ³J_{FC} = 4.0, C2), 136.2 (br d, ³J_{FC} = 4.3, C2'), 134.6 (d, ³J_{FC} = 12.5, C8), 129.8 (d, ⁴J_{FC} = 11.0, C9), 126.8 (d, ¹J_{FC} = 56.0, C7), 122.5 (s, C4), 121.5 (s, C4'), 120.0 (d, ⁴J_{FC} = 6.5, C5), 119.4 (s, C5'), 34.3 (s, CMe₃), 34.1 (s, CMe₃'), 31.0 (s, CMe₃), 30.4 (s, CMe₃'), 20.6 ppm (s, Me). ³¹P{¹H} NMR (121.49 MHz, THF-*d*₆, 213 K): 32.6 ppm (s, Ptol₃). ¹H NMR (300.13 MHz, Toluene-*d*₈, 298K, *J* values in Hz): δ 8.60 (br d, ⁴J_{HP} = 9.7, 1H, H2), 7.58 (m, 2H, H5+H5'), 7.51 (dd, ³J_{HP} = 12.3, ³J_{HH} = 8.2, 6H, H8), 7.25 (m, 2H, H2'+H4), 7.15 (dd, ³J_{HH} = 8.2, ⁴J_{HH} = 1.5, 1H, H4'), 6.79 (d, ³J_{HH} = 8.2, 6H, H9), 2.94 (br d, ²J_{HP} = 32.4, 1H, Au-H), 1.98 (s, 9H, Me), 1.38 (s, 9H, CMe₃), 1.02 ppm (s, 9H, CMe₃').

(C[∧]C)AuH(PPh₃) (11). This complex was synthesized by following the procedure reported for (C[∧]C)AuH(PMe₃), by using 15 mg of **2**, 26 μL of LiHBET₃ and 1.0 equivalent of PPh₃ (6.8 mg) in dry THF-*d*₆. NMR characterization was carried out at 298K. ¹H NMR (300.13 MHz, THF-*d*₆, 298 K, *J* values in Hz): δ 8.02 (brd, ⁴J_{HP} = 9.7, 1H, H2), 7.66 (m, overlapped with py signals, H8), 7.50 (m, 9H, H9+H10), 7.30 (m, 2H, H5+H5'), 7.09 (brd, ³J_{HH} = 8.3, 1H, H4), 7.05 (brs, 1H, H2'), 6.92 (brd, ³J_{HH} = 8.3, 1H, H4'), 2.40 (brd, ²J_{HP} = 32.3, 1H, Au-H), 1.29 (s, 9H, CMe₃), 0.81 ppm (s, 9H, CMe₃'). ¹³C{¹H} NMR (75.47 MHz, THF-*d*₆, 298 K, *J* values in Hz): δ 169.3 (d, ²J_{FC} = 5.1, C1'), 160.5 (d, ²J_{FC} = 129.5, C1), 154.5 (d, ³J_{FC} = 5.2, C6), 154.1 (s, C6'), 149.8 (d, ⁴J_{FC} = 9.4, C3), 148.8 (s, C3'), 140.9 (d, ³J_{FC} = 4.7, C2), 136.5 (d, ³J_{FC} = 5.5, C2'), 135.4 (d, ³J_{FC} = 12.6, C8), 132.2 (br s, C10), 131.0 (d, ¹J_{CP} = 49.9, C7), 129.7 (d, ⁴J_{FC} = 10.9, C9), 123.3 (s, C4), 122.5 (s, C4'), 120.8 (d, ⁴J_{FC} = 7.2, C5), 120.2 (s, C5'), 34.9 (s, CMe₃), 34.6 (s, CMe₃'), 31.7 (s, CMe₃), 31.4 ppm (s, CMe₃'). ³¹P{¹H} NMR (121.49 MHz, THF-*d*₆, 298 K): 34.9 ppm (s, PPh₃).

(C[∧]C)Au(Z-C₂H(CO₂Me)₂)(PMe₃) (12). A sample of **9** was generated from 15 mg of **2** in THF-*d*₆ and treated with 2 equiv

DMAD at room temperature. The conversion to the vinyl complex was complete in 2h. NMR characterization was performed in mixture with py-BEt₃, at 298K. ¹H NMR (300.13 MHz, THF-*d*₆, 298 K, *J* values in Hz): δ 7.54 (m, 3H, H₂+H₂' +H₈), 7.32 (d, ³*J*_{HH} = 8.2, 1H, H₅'), 7.23 (dd, ³*J*_{HH} = 8.2 ⁵*J*_{HF} = 3.8, 1H, H₅), 7.11 (dd, ³*J*_{HH} = 8.2 ⁴*J*_{HH} = 1.9, 1H, H₄'), 7.01 (dd, ³*J*_{HH} = 8.2 ⁴*J*_{HH} = 1.7, 1H, H₄), 3.68 (s, 3H, H₁₀), 3.59 (buried under THF, H₁₂), 1.78 (buried under THF, PMe₃'), 1.34 (s, 9H, CMe₃'), 1.24 ppm (s, 9H, CMe₃'). ¹³C{¹H} NMR (75.47 MHz, THF-*d*₆, 298 K, *J* values in Hz): δ 184.1 (d, ²*J*_{CP} = 14.8, C7), 173.4 (s, C9), 170.0 (s, C11), 159.5 (d, ²*J*_{CP} = 138.0, C1), 158.7 (s, C1'), 153.3 (d, ³*J*_{CP} = 5.1, C6), 152.2 (s, C6'), 148.1 (d, ⁴*J*_{CP} = 9.4, C3), 147.8 (s, C3'), 131.7 (d, ³*J*_{CP} = 3.5, C2'), 131.6 (d, ³*J*_{CP} = 9.0, C2), 127.1 (d, ³*J*_{CP} = 3.0, C8), 122.6 (s, C4+C4'), 120.2 (s, C5'), 119.9 (d, ⁴*J*_{CP} = 7.4, C5), 51.0 (s, C10), 50.6 (s, C12), 34.5 (s, CMe₃), 34.3 (s, CMe₃'), 31.1 (s, CMe₃'), 30.8 (s, CMe₃), 13.1 ppm (d, ¹*J*_{CP} = 31.7, PMe₃). ³¹P{¹H} NMR (121.49 MHz, THF-*d*₆, 298 K): -5.6 ppm (s, PMe₃).

(C[∞]C)Au(ZC₂H(CO₂Me)₂)(Ptol₃) (13). A sample of **10** was generated from 15 mg of **2** in THF-*d*₆ and treated with 2 equiv DMAD at room temperature. The conversion into the vinyl complex was complete in 12h, affording **13** in 80% yield. NMR characterization was performed in mixture with py-BEt₃, at 298 K. ¹H NMR (300.13 MHz, THF-*d*₆, 298 K, *J* values in Hz): δ 7.65 (br, overlapped with pyridine signals, H₁₄), 7.42 (dd, 1H, ⁴*J*_{HF} = 9.5, ⁴*J*_{HH} = 1.6, H₂'), 7.2 (m, 6H, H₁₅), 7.06 (m, 2H, H₄' +H₈), 6.95 (br t, 1H, H₂), 6.88 (dd, ³*J*_{HH} = 8.0, ⁴*J*_{HH} = 1.7, H₂'), 3.46 (s, 3H, H₁₀), 3.43 (s, 3H, H₁₂), 2.35 (s, 9H, PhMe), 1.20 (s, 9H, CMe₃), 0.65 ppm (s, 9H, CMe₃'). Partial ¹³C{¹H} NMR (75.47 MHz, THF-*d*₆, 298 K, *J* values in Hz): δ 186.0 (d, ²*J*_{CP} = 13.3, C7), 172.1 (s, C9), 169.2 (s, C11), 159.6 (d, ²*J*_{CP} = 126.3, C1), 159.3 (d, ²*J*_{CP} = 6.3, C1'), 152.8 (d, ⁴*J*_{CP} = 4.0, C6'), 152.6 (s, C6), 148.2 (d, ⁴*J*_{CP} = 8.7, C3), 147.2 (s, C3'), 141.5 (s, C16), 137.0 (d, ³*J*_{CP} = 8.8, C2'), 135.3 (br, C14), 131.7 (d, ³*J*_{CP} = 2.4, C2), 129.1 (brs, C8), 128.7 (d, ³*J*_{CP} = 12.4, C15), 126.8 (d, ¹*J*_{CP} = 49.8, C7), 122.7 (s, C4), 121.5 (s, C4'), 119.9 (d, ⁴*J*_{CP} = 6.9, C5), 119.2 (s, C5'), 50.5 (s, C10), 50.2 (s, C12), 34.5 (s, CMe₃), 33.8 (s, CMe₃'), 30.8 (s, CMe₃), 30.3 (s, CMe₃'), 20.4 ppm (s, (C16)Me). ³¹P{¹H} NMR (121.49 MHz, THF-*d*₆, 298 K): 33.2 ppm (s, Ptol₃).

Li[(C[∞]C)AuH₂] (14). A solution of **10** in THF-*d*₆ was generated from 15 mg of **2** as described above. Successively, a second equivalent of LiHBET₃ was added to the solution at room temperature and the slow conversion of the monohydride to the dihydride anion was observed, with liberation of free Ptol₃. ¹H NMR (300.13 MHz, THF-*d*₆, 298 K, *J* values in Hz): δ 8.00 (m, 2H, H₂), 7.17 (d, ³*J*_{HH} = 8.1, 2H, H₅), 6.86 (dd, ³*J*_{HH} = 8.1 ⁴*J*_{HH} = 2.2, 2H, H₄), 1.27 (s, 18H, CMe₃), 0.09 ppm (ps t, ⁴*J*_{HH} = 2.3, 2H, Au-H). ¹³C{¹H} NMR (75.47 MHz, THF-*d*₆, 298 K): δ 170.7 (s, C1), 156.2 (s, C6), 147.7 (s, C3), 140.2 (s, C2), 120.3 (s, C4), 119.2 (s, C5), 34.6 (s, CMe₃), 32.0 ppm (s, CMe₃'). ¹H NMR (300.13 MHz, Toluene-*d*₆, 298 K, *J* values in Hz): δ 8.36 (m, 2H, H₂), 7.55 (d, ³*J*_{HH} = 8.1, 2H, H₅), 7.20 (dd, ³*J*_{HH} = 8.1 ⁴*J*_{HH} = 2.0, 2H, H₄), 1.41 (s, 18H, CMe₃), 1.00 ppm (ps t, ⁴*J*_{HH} = 2.3, 2H, Au-H).

[NBu₄][(C[∞]C)Au(H)C₆F₅] (16). *Procedure (a):* In the glovebox, 15 mg of [NBu₄][(C[∞]C)Au(Cl)C₆F₅] (**15**) were loaded into a screw cap NMR tube and dissolved in approximately 0.7 ml of THF-*d*₆. Successively, 1.2 equivalents of LiHBET₃ were added at 195K and the sample was then allowed to warm up at room temperature. The reaction went to completion in 24h at room temperature. *Procedure (b):* In the glovebox, 20 mg of **15** were loaded into

a screw-cap NMR tube and suspended in approximately 0.7 mL of toluene-*d*₆. Successively, 1.2 equiv LiHBET₃ were added at room temperature to afford a pale-yellow solution with an off-white precipitate. The solution was filtered into a J-young NMR tube, dried under vacuum and re-dissolved in THF-*d*₆. ¹H NMR (300.13 MHz, THF-*d*₆, 298 K, *J* values in Hz): δ 8.07 (m, 1H, H₂), 7.26 (d, ³*J*_{HH} = 8.1, 1H, H₅), 7.23 (d, ³*J*_{HH} = 8.1, 1H, H₅'), 7.09 (m, 1H, H₂'), 7.00 (dd, ³*J*_{HH} = 8.1 ⁴*J*_{HH} = 2.2, 1H, H₄), 6.94 (dd, ³*J*_{HH} = 8.1 ⁴*J*_{HH} = 2.2, 1H, H₄'), 2.91 (m, 8H, H_α), 1.35 (br m, 8H, H_β), 1.32 (s, 9H, CMe₃), 1.23 (q, ³*J*_{HH} = 7.8, H_γ), 1.15 (overlapped with CMe₃', Au-H), 1.14 (s, 9H, CMe₃'), 0.90 ppm (t, 12H, ³*J*_{HH} = 7.8, H_δ). ¹³C{¹H} NMR (75.47 MHz, THF-*d*₆, 298 K): δ 170.3 (s, C1'), 160.1 (brs, C1), 155.3 (s, C6'), 154.3 (s, C6), 148.8 (s, C3'), 148.0 (s, C3), 141.1 (s, C2'), 133.1 (s, C2), 121.8 (s+s, C4+C4'), 119.9 (s, C5'), 119.6 (s, C5), 58.8 (s, C_α), 34.8 (s, CMe₃+CMe₃'), 31.8 (s, CMe₃), 31.7 (s, CMe₃'), 24.2 (s, C_β), 20.2 (s, C_γ), 13.8 ppm (s, C_δ). ¹⁹F NMR (282.4 MHz, THF-*d*₆, 298 K, *J* values in Hz): -116.6 (m, ³*J*_{FF} = 23.0, 2F, *o*-F), -165.6 (m, 3F, *p*-F+*m*-F). ¹H NMR (300.13 MHz, Toluene-*d*₆, 298 K, *J* values in Hz): δ 8.31 (s, 1H, H₂), 7.41 (br s, 1H, H₂'), 7.34 (m, 2H, H₅+H₅'), 7.04 (m, partially overlapped with toluene, H₄+H₄'), 2.47 (br m, 8H, H_α), 1.67 (brs, 1H, Au-H), 1.39 (s, 9H, CMe₃), 1.32 (brm, partially overlapped with THF and BEt₃, H_β), 1.23 (s, 9H, CMe₃'), 0.99 (brm, partially overlapped with BEt₃, H_γ), 0.83 ppm (brt, ³*J*_{HH} = 7.3, 9H, H_δ).

[NBu₄][(C[∞]C)Au(ZC₂H(CO₂Me)₂)C₆F₅] (17). A sample of [NBu₄][(C[∞]C)Au(H)C₆F₅] was generated from 10 mg of (C[∞]C)AuCl(py) in THF-*d*₆ and treated with 2 equivalents of DMAD at room temperature to give a bright orange solution. Conversion into the vinyl product was instantaneous, as indicated by ¹H NMR. The THF solution was then passed through silica, dried and washed with light petroleum ether to remove most of borane and DMAD impurities. ¹H NMR (300.13 MHz, THF-*d*₆, 298 K, *J* values in Hz): δ 7.59 (d, ⁴*J*_{HH} = 2.1, 1H, H₂), 7.26 (s, 1H, H₈), 7.21 (m, 2H, H₅+H₅'), 6.97 (m, 3H, H₂' +H₄+H₄'), 3.52 (s, 3H, H₁₀), 3.48 (s, 3H, H₁₂), 3.02 (m, 8H, H_α), 1.43 (m, 8H, H_β), 1.23 (s, 9H, CMe₃), 1.19 (q, 8H, ³*J*_{HH} = 7.4, H_γ), 1.13 (s, 9H, CMe₃'), 0.9 ppm (t, 9H, ³*J*_{HH} = 7.4, H_δ). ¹³C{¹H} NMR (75.47 MHz, THF-*d*₆, 298 K): δ 184.7 (s, C7), 175.0 (s, C9), 169.2 (s, C11), 159.8 (s, C1'), 159.2 (brs, C1), 153.3 (s, C6'), 152.7 (s, C6), 147.6 (s, C3), 147.2 (s, C3'), 132.8 (s, C2'), 132.4 (s, C2), 126.4 (s, C8), 121.6 (s, C4), 121.1 (s, C4'), 119.2 (s, C5'), 118.8 (s, C5), 57.7 (s, C_α), 50.1 (s, C10), 49.8 (s, C12), 34.4 (s, CMe₃), 34.0 (s, CMe₃'), 31.0 (s, CMe₃), 30.9 (s, CMe₃'), 23.6 (s, C_β), 19.4 (s, C_γ), 13.1 ppm (s, C_δ). ¹⁹F NMR (282.4 MHz, THF-*d*₆, 298 K, *J* values in Hz): -116.4 (dm, ³*J*_{FF} = 34.1, 1F, *o*-F), -117.2 (dm, ³*J*_{FF} = 34.1, 1F, *o*-F), -165.2 (t, ³*J*_{FF} = 19.8, 1F, *p*-F), -166.0 (m, 2H, *o*-F). ¹H NMR (300.13 MHz, CD₂Cl₂, 298 K, *J* values in Hz): δ 7.58 (d, ⁴*J*_{HH} = 1.6, 1H, H₂), 7.28 (m, 3H, H₅+H₅' +H₈), 7.04 (dd, ³*J*_{HH} = 8.1 ⁴*J*_{HH} = 1.8, 2H, H₄+H₄'), 3.6 (s, 3H, H₁₂), 3.54 (s, 3H, H₁₀), 2.85 (m, H_α), 1.33 (m, H_β), 1.24 (s, 9H, CMe₃), 1.18 (m, H_γ), 1.13 (s, 9H, CMe₃'), 0.91 ppm (t, ³*J*_{HH} = 7.3, H_δ).

Li[(C[∞]C)Au(ZC₂H(CO₂Me)CH₂OBEt₃(PMe₃))] (18). A sample of **12** was generated *in situ* in THF-*d*₆ and treated at room temperature with aliquots of LiHBET₃ until reaching a Au/hydride stoichiometric ratio of 2.5. Full conversion of **12** into **18** was observed immediately. ¹H NMR (300.13 MHz, THF-*d*₆, 298 K, *J* values in Hz): δ 7.93 (m, 1H, H₈), 7.62 (dd, ⁴*J*_{PH} = 9.7, ⁴*J*_{HH} = 1.6, 1H,

H2), 7.55 (brs, 1H, H2'), 7.32 (d, $^3J_{\text{HH}} = 8.1$, 1H, H5'), 7.25 (dd, $^3J_{\text{HH}} = 8.0$, $^5J_{\text{FH}} = 4.1$, 1H, H5), 7.09 (dd, $^3J_{\text{HH}} = 8.1$, $^4J_{\text{HH}} = 1.6$, 1H, H4'), 7.03 (br d, $^3J_{\text{HH}} = 8.0$, 1H, H4), 3.01 (br d, $^3J_{\text{HH}} = 4.3$, 2H, H9), 3.59 (buried under THF, H11), 1.81 (partially overlapped with THF, PMe_3), 1.33 (s, 9H, CMe_3 '), 1.24 (s, 9H, CMe_3), 0.66 (br t, overlapped with BEt_3 , $\text{O}-\text{BCH}_2\text{CH}_3$), 0.00 ppm (br t, overlapped with BEt_3 , $\text{O}-\text{BCH}_2\text{CH}_3$). $^{13}\text{C}\{^1\text{H}\}$ NMR (75.47 MHz, THF- d_6 , 298 K, J values in Hz): δ 174.0 (s, C7), 163.2 (d, $^2J_{\text{PC}}=6.2$, C1'), 159.8 (d, $^2J_{\text{PC}}=138.7$, C1), 159.7 (d, $^3J_{\text{PC}}=14.6$, C10), 154.2 (d, $^3J_{\text{PC}} = 5.4$, C6'), 153.6 (s, C6), 149.9 (s, C8), 148.6 (s, C3'), 148.5 (s, $^4J_{\text{FC}} = 9.9$, C3), 132.5 (d, $^3J_{\text{FC}} = 7.1$, C2'), 132.4 (s, C2), 123.4 (s, C4), 123.2 (s, C4'), 120.6 (m, C5+C5'), 64.7 (s, C9), 51.1 (s, C11), 35.2 (s, CMe_3), 35.1 (s, CMe_3 '), 31.8 (s, CMe_3 '), 31.7 (s, CMe_3), 14.0 (d, $^1J_{\text{FC}} = 31.6$, PMe_3), 13.9 (brs, overlapped with PMe_3 , $\text{O}-\text{BCH}_2\text{CH}_3$), 10.9 ppm (overlapped with BEt_3 , $\text{O}-\text{BCH}_2\text{CH}_3$).

Z-dimethyl(3-butyl(6-(4-butylphenyl)phenyl)fumarate) (19).

A sample of **12** was generated in THF- d_6 and treated at room temperature with sub-stoichiometric portions of $[\text{H}(\text{OEt})_2][\text{H}_2\text{N}-\{\text{B}(\text{C}_6\text{F}_5)_3\}_2]$ until reacting a stoichiometric ratio of acid/Au of 1.2. Upon addition of the acid, the deep orange colour of **12** faded to give a pale yellow solution and the formation of a dark precipitate. ^1H NMR spectroscopy revealed the complete disappearance of **12** to give **19** in 65% yield. NMR characterization is given in mixture.

^1H NMR (300.13 MHz, THF- d_6 , 298 K, J values in Hz): δ 7.43 (dd, $^3J_{\text{HH}} = 8.1$, $^4J_{\text{HH}} = 2.0$, 1H, H4), 7.34 (d, $^3J_{\text{HH}} = 8.5$, 2H, H4'), 7.24 (m, 2H, H5+H8), 7.20 (d, $^3J_{\text{HH}} = 8.5$, 2H, H5'), 6.83 (s, H8), 3.54 (s, 3H, H12), 3.3 (s, 3H, H10), 1.34 (s, 9H, CMe_3), 1.32 ppm (s, 9H, CMe_3 '). Partial $^{13}\text{C}\{^1\text{H}\}$ NMR (75.47 MHz, THF- d_6 , 298 K): δ 165.8 (s, C9), 165.4 (s, C11), 149.7 (overlapped with AB_2 , C3'), 149.4 (s, C3), 138.8 (overlapped with AB_2 , C6'+C6), 133.0 (s, C1), 128.9 (s, C8), 128.8 (s, C5), 128.7 (s, C5'), 127.3 (s, C8), 125.4 (s, C4), 124.5 (s, C4'), 51.2 (s, C10), 50.8 (s, C12), 34.7 (s+s, $\text{CMe}_3+\text{CMe}_3$ '), 30.7 ppm (s, $\text{CMe}_3+\text{CMe}_3$ ').

$[(\text{C}^{\wedge}\text{N}-\text{CH})\text{AuH}(\mu\text{-H})\text{Au}(\text{C}^{\wedge}\text{N}^{\wedge}\text{C})][\text{AB}_2]$ (**20**). Within the glovebox, 15 mg of $(\text{C}^{\wedge}\text{N}^{\wedge}\text{C})\text{AuH}$ were loaded into a screw-cap NMR tube and dissolved in approximately 0.3 mL of dry CD_2Cl_2 . 1 equiv $[\text{H}(\text{OEt})_2][\text{H}_2\text{N}\{\text{B}(\text{C}_6\text{F}_5)_3\}_2]$ (33.1 mg, 0.028 mmol) was dissolved in 0.4 mL of dry CD_2Cl_2 and loaded into a gas-tight syringe equipped with a rubber stopper. Outside the glovebox, the NMR tube was inserted into a cold bath at 198K and the acid solution was slowly injected through the septum at low temperature. The sample was then shaken quickly, inserted in the pre-cooled NMR probe and studied at 213 K. Extensive decomposition was observed after 1 h at 213 K. ^1H NMR (300.13 MHz, CD_2Cl_2 , 213 K, J values in Hz): δ 8.23 (t, $^3J_{\text{HH}} = 8.0$, 1H, H1), 8.08 (d, $^3J_{\text{HH}} = 8.0$, 1H, H2), 7.79 (m, 3H, H5+H2'+H1a), 7.60 (m, 2H, H6+H8), 7.38 (m, 8H, H5'+H2a+H5a+H6a), 7.17 (m, 4H, H6'+H8a), 5.56 (br s, NH_2), 1.13 (s, 9H, CMe_3), 1.03 (s, 18H, CMe_3a), 0.81 (s, 9H, CMe_3 '), -4.93 (d, $^2J_{\text{HH}} = 8.6$, 1H, Hb), -8.47 ppm (br d, $^2J_{\text{HH}} = 8.6$, 1H, Ha).

$[(\text{C}^{\wedge}\text{N}-\text{CH})\text{AuMe}(\mu\text{-H})\text{Au}(\text{C}^{\wedge}\text{N}^{\wedge}\text{C})][\text{AB}_2]$ (**21**). 10 mg of $(\text{C}^{\wedge}\text{N}^{\wedge}\text{C})\text{AuMe}$ and 1.0 equivalents of $[\text{H}(\text{OEt})_2][\text{H}_2\text{N}-\{\text{B}(\text{C}_6\text{F}_5)_3\}_2]$ were loaded within a screw cap NMR and dissolved in approximately 0.5 mL of CD_2Cl_2 . Outside the glovebox, the NMR sample was inserted in a cold bath at 195 K and 1.0 equiv $(\text{C}^{\wedge}\text{N}^{\wedge}\text{C})\text{AuH}$ (9.7 mg, 0.018 mmol, dissolved in 0.3 ml of

CD_2Cl_2) were injected through the septum to give a bright yellow solution, which was quickly shaken and inserted into the pre-cooled NMR probe at 213 K. **21** was observed in 65% yield, along with unreacted **3a**. Partial ^1H NMR (300.13 MHz, CD_2Cl_2 , 243 K, J values in Hz): 8.21 (m, 2H, H1+H2), 7.89 (m, 2H, H1a+H2'), 7.72 (br d, overlapped with **3a**, H5), 7.50 (br d, $^3J_{\text{HH}} = 8.1$, 1H, H6), 7.43 (m, 6H, H2a+H5a+H5'), 7.34 (br s, 4H, H8a+H6'), 7.27 (s, overlapped with **3a**, H8), 7.20 (d, $^3J_{\text{HH}} = 8.1$, H6a), 5.62 (br s, NH_2), 1.71 (s, 3H, Au-Me), 1.26 (s, 9H, CMe_3), 1.08 (s, overlapped with Et_2O , CMe_3a), 0.76 (s, 9H, CMe_3 '), -5.14 ppm (s, 1H, Au-H-Au).

$[(\text{C}^{\wedge}\text{N}-\text{CH})\text{AuMe}(\mu\text{-H})\text{MeAu}(\text{C}^{\wedge}\text{N}-\text{CH})][\text{AB}_2]$ (**22a**). 15 mg of $(\text{C}^{\wedge}\text{N}^{\wedge}\text{C})\text{AuMe}$ and 1.0 equivalents of $[\text{H}(\text{OEt})_2][\text{H}_2\text{N}-\{\text{B}(\text{C}_6\text{F}_5)_3\}_2]$ were loaded within a screw cap NMR and dissolved in approximately 0.6 ml of CD_2Cl_2 . Outside the glovebox, the NMR sample was inserted in a cold bath at 195 K and 5.0 equivalents of $\text{HSi}(\text{OMe})_3$ were injected through the septum. The sample was quickly shaken and inserted in the pre-cooled NMR probe at 243 K. ^1H NMR (300.13 MHz, CD_2Cl_2 , 243 K, J values in Hz): δ 8.18 (t, $^3J_{\text{HH}} = 7.8$, 2H, H1), 8.06 (d, $^3J_{\text{HH}} = 7.8$, 2H, H2), 7.76 (d, $^3J_{\text{HH}} = 8.2$, 2H, H5), 7.46 (d, $^3J_{\text{HH}} = 7.8$, 2H, H2'), 7.42 (d, $^3J_{\text{HH}} = 8.2$, 2H, H6), 7.33 (br m, 4H, H8+H6'a), 7.21 (d, $^3J_{\text{HH}} = 8.4$, 2H, H5'a), 6.77 (d, $^3J_{\text{HH}} = 8.2$, 2H, H6'b), 6.55 (d, $^3J_{\text{HH}} = 8.2$, 2H, H5'b), 5.66 (br s, 2H, NH_2), 1.35 (s, 3H, Au-Me), 1.31 (s, 18H, CMe_3), 0.75 (s, 18H, CMe_3 '), -2.53 ppm (s, 1H, Au-H-Au). $^{13}\text{C}\{^1\text{H}\}$ NMR (75.47 MHz, CD_2Cl_2 , 223 K, J values in Hz): δ 161.2 (s, C3), 160.3 (s, C3'), 154.9 (s, C7), 154.1 (s, C9), 153.5 (s, C7'), 147.5 (br d, $^1J_{\text{CF}} = 238.5$, $\text{o}-\text{F}$ $\text{H}_2\text{N}[\text{B}(\text{C}_6\text{F}_5)_3]_2^-$), 141.8 (s, C1), 141.2 (s, C4), 138.9 (br d, $^1J_{\text{CF}} = 250.0$, $\text{p}-\text{F}$ $\text{H}_2\text{N}[\text{B}(\text{C}_6\text{F}_5)_3]_2^-$), 136.5 (br d, $^1J_{\text{CF}} = 250.0$, $\text{m}-\text{F}$ $\text{H}_2\text{N}[\text{B}(\text{C}_6\text{F}_5)_3]_2^-$), 137.2 (s, C4'), 130.7 (s, C5'a), 127.2 (s, C8+C5), 126.2 (s, C6), 125.7 (s+s, C5'b+C6'a), 125.2 (s, C6'b), 124.4 (s, C2'), 118.8 (s, C2), 35.7 (s, CMe_3), 34.3 (s, CMe_3 '), 30.9 (s, CMe_3), 30.2 (s, CMe_3 '), 10.0 ppm (s, Au-Me).

$[(\text{C}^{\wedge}\text{N}-\text{CH})\text{AuC}_6\text{F}_5(\mu\text{-H})\text{Au}(\text{F}_3\text{C}_6)(\text{C}^{\wedge}\text{N}-\text{CH})][\text{AB}_2]$ (**22b**). 15 mg of $(\text{C}^{\wedge}\text{N}^{\wedge}\text{C})\text{AuC}_6\text{F}_5$ and 1.0 equiv $[\text{H}(\text{OEt})_2][\text{H}_2\text{N}-\{\text{B}(\text{C}_6\text{F}_5)_3\}_2]$ were loaded within a screw-cap NMR and dissolved in approximately 0.6 mL of CD_2Cl_2 . Outside the glovebox, the NMR sample was inserted in a cold bath at 195 K and 5.0 equiv $\text{HSi}(\text{OMe})_3$ were injected through the septum. The sample was quickly shaken and inserted in the pre-cooled NMR probe at 223 K. ^1H NMR (300.13 MHz, CD_2Cl_2 , 223 K, J values in Hz): δ 8.34 (t, $^3J_{\text{HH}} = 7.8$, 2H, H1), 8.13 (d, $^3J_{\text{HH}} = 7.8$, 2H, H2), 7.78 (d, $^3J_{\text{HH}} = 8.2$, 2H, H5), 7.56 (d, $^3J_{\text{HH}} = 7.8$, 2H, H2'), 7.50 (m, 4H, H5'a+H6'a), 7.38 (d, $^3J_{\text{HH}} = 8.2$, 2H, H6), 7.07 (d, $^3J_{\text{HH}} = 8.3$, 2H, H6'b), 6.33 (d, $^3J_{\text{HH}} = 8.3$, 2H, H5'b), 6.07 (s, 2H, H8), 5.64 (br s, 4H, NH_2), 1.00 (s, 18H, CMe_3), 0.82 (s, 18H, CMe_3 '), -2.21 ppm (s, 1H, Au-H-Au). $^{13}\text{C}\{^1\text{H}\}$ NMR (75.47 MHz, CD_2Cl_2 , 223 K, J values in Hz): δ 162.2 (s, C3), 160.3 (s, C3'), 159.5 (s, C9), 156.5 (s, C7), 154.8 (s, C7'), 147.5 (br d, $^1J_{\text{CF}} = 239.8$, $\text{o}-\text{F}$ $\text{H}_2\text{N}[\text{B}(\text{C}_6\text{F}_5)_3]_2^-$), 143.3 (s, C1), 138.9 (s, C4), 138.8 (br d, $^1J_{\text{CF}} = 250.0$, $\text{p}-\text{F}$ $\text{H}_2\text{N}[\text{B}(\text{C}_6\text{F}_5)_3]_2^-$), 136.4 (br d, $^1J_{\text{CF}} = 250.0$, $\text{m}-\text{F}$ $\text{H}_2\text{N}[\text{B}(\text{C}_6\text{F}_5)_3]_2^-$), 134.9 (s, C4'), 130.0 (s, C5'a), 129.4 (s, C8), 128.2 (s, C5), 127.9 (s, C6'a), 127.5 (s, C6'b), 127.2 (s, C6), 126.2 (s, C2'), 125.7 (s, C5'b), 119.5 (s, C2), 35.5 (s, CMe_3), 34.7 (s, CMe_3 '), 30.5 (s, CMe_3), 29.9 ppm (s, CMe_3 '). ^{19}F NMR (282.4 MHz, CD_2Cl_2 , 223 K, J values in Hz): -118.2 (dq, $^3J_{\text{FF}} = 25.7$ $^4J_{\text{FF}} = 6.0$, 1F, $\text{o}-\text{F}$ Au- C_6F_5), -119.7 (d ps t, $^3J_{\text{FF}} = 27.7$ $^4J_{\text{FF}} = 6.4$, 1F, $\text{o}-\text{F}$ Au- C_6F_5), -133.2 (br s, 12F, $\text{o}-\text{F}$ $\text{H}_2\text{N}[\text{B}(\text{C}_6\text{F}_5)_3]_2^-$), -154.8 (t, $^3J_{\text{FF}} = 21.0$, 1F, $\text{p}-\text{F}$ Au- C_6F_5), -159.4 (t, $^3J_{\text{FF}} = 21.1$, 1F, $\text{p}-\text{F}$ $\text{H}_2\text{N}[\text{B}(\text{C}_6\text{F}_5)_3]_2^-$), -160.1 (m, 1F, $\text{m}-\text{F}$ Au-

C₆F₅), -164.9 ppm (brm, 13F, *m*-F Au-C₆F₅ + *m*-F H₂N[B(C₆F₅)₃]₂⁻).

ASSOCIATED CONTENT

Supporting Information

The Supporting Information is available free of charge via the Internet at <http://pubs.acs.org>: Experimental details, characterization, crystallographic data, NMR spectra, and computational details (PDF); Cartesian coordinates of the selected DFT optimized structures (XYZ); X-ray crystallographic details (CIF)

AUTHOR INFORMATION

Corresponding Authors

*lrocchigiani@uea.ac.uk
 *peter.hrobarik@uniba.sk
 *m.bochmann@uea.ac.uk

ORCID

Luca Rocchigiani: 0000-0002-2679-8407
 Julio Fernandez-Cestau 0000-0001-7663-6222
 Isabelle Chambrier: 0000-0003-0090-1186
 Peter Hrobárik: 0000-0002-6444-8555
 Manfred Bochmann: 0000-0001-7736-5428

Author Contributions

All authors have given approval to the final version of the manuscript.

Note

The authors declare no conflict of interest.

ACKNOWLEDGMENT

This work was supported by the European Research Council. M.B. is an ERC Advanced Investigator Award holder (grant no. 338944-GOCAT). P. H. gratefully acknowledges support from the Berlin DFG excellence cluster on Unifying Concepts in Catalysis (UniCat) as well as funding from the Slovak VEGA grant agency (grants no. 1/0507/17 and 1/0712/18) and from the European Union's Horizon 2020 research and innovation programme under the Marie Skłodowska-Curie Grant Agreement No.752285. We thank Prof. Cristina Nevado for helpful discussions. We are grateful to the EPSRC National Crystallographic Service, Southampton, UK, for collection of crystallographic data sets.⁴¹

REFERENCES

- (1) (a) Norton, J. R.; Sowa, J. R. *Chem. Rev.* **2016**, *116*, 8315–8317. (b) *Chem. Rev.* **2016**, *116*, 8315–9000 (themed issue).
- (2) Schmidbaur, H.; Raubenheimer, H. G.; Dobrzańska, L. *Chem. Soc. Rev.* **2014**, *43*, 345–380.
- (3) (a) Wang, X.; Andrews, L. *J. Am. Chem. Soc.* **2001**, *123*, 12899–12900. (b) Wang, X.; Andrews, L. *Angew. Chem. Int. Ed.* **2003**, *42*, 5201–5206. (c) Andrews, L.; Wang, X. *J. Am. Chem. Soc.* **2003**, *125*, 11751–11760. (d) Andrews, L. *Chem. Soc. Rev.* **2004**, *33*, 123–132.
- (4) Tsui, E. Y.; Müller, P.; Sadighi, J. P. *Angew. Chem. Int. Ed.* **2008**, *47*, 8937–8940. Hydride-bridged binuclear gold(I) phosphine complexes have also been reported: Escalle, A.; Mora, G.; Gagosz, F.; Mézailles, N.; Le Goff, X. F.; Jean, Y.; Le Floch, P. *Inorg. Chem.* **2009**, *48*, 8415–8422.
- (5) Roşca, D.-A.; Smith, D. A.; Hughes, D. L.; Bochmann, M. *Angew. Chem. Int. Ed.* **2012**, *51*, 10643–10646.
- (6) Pintus, A.; Rocchigiani, L.; Fernandez-Cestau, J.; Budzelaar, P. H. M.; Bochmann, M. *Angew. Chem. Int. Ed.* **2016**, *55*, 12321–12324.
- (7) Kleinhans, G.; Hansmann, M. M.; Guisado-Barrios, G.; Liles, D. C.; Bertrand, G.; Bezuidenhout, D. I. *J. Am. Chem. Soc.* **2016**, *138*, 15873–15876.

- (8) (a) Roşca, D.-A.; Wright, J. A.; Hughes, D. L.; Bochmann, M. *Nature Commun.* **2013**, *4*, 2167. (b) Roşca, D.-A.; Fernandez-Cestau, J.; Morris, J.; Wright, J. A.; Bochmann, M. *Science Adv.* **2015**, *1*, e1500761.
- (9) Reviews: (a) Roşca, D.-A.; Wright, J. A.; Bochmann, M. *Dalton Trans.* **2015**, *44*, 20785–20807. (b) Kumar, R.; Nevado, C. *Angew. Chem. Int. Ed.* **2017**, *56*, 1994–2015.
- (10) Pintus, A.; Bochmann, M. *RSC Adv.* **2018**, *8*, 2795–2803.
- (11) (a) Joost, M.; Amgoune, A.; Bourissou, D. *Angew. Chem., Int. Ed.* **2015**, *54*, 15022–15045. (b) Rekhroukh, F.; Estevez, L.; Mallet-Ladeira, S.; Miqueu, K.; Amgoune, A.; Bourissou, D. *J. Am. Chem. Soc.* **2016**, *138*, 11920–11929.
- (12) (a) Comas-Vives, A.; González-Arellano, C.; Corma, A.; Iglesias, M.; Sánchez, F.; Ujaque, G. *J. Am. Chem. Soc.* **2006**, *128*, 4756–4765. (b) Casado, R.; Contel, M.; Laguna, M.; Romero, P.; Sanz, S. *J. Am. Chem. Soc.* **2003**, *125*, 11925–11935. (c) Lv, H.; Zhan, J.-H.; Cai, Y.-B.; Yu, Y.; Wang, B.; Zhang, J.-L. *J. Am. Chem. Soc.* **2012**, *134*, 16216–16227.
- (13) (a) Klatt, G.; Xu, R.; Pernpointner, M.; Molinari, L.; Hung, T. Q.; Rominger, F.; Hashmi, A. S. K.; Köppel, H. *Chem. Eur. J.* **2013**, *19*, 3954–3961. (b) Ung, G.; Bertrand, G. *Angew. Chem., Int. Ed.* **2013**, *52*, 11388–11391. (c) Reis, M. C.; López, C. S.; Kraka, E.; Cremer, D.; Faza, O. N. *Inorg. Chem.* **2016**, *55*, 8636–8645.
- (14) Kumar, R.; Krieger, J.-P.; Gómez-Bengo, E.; Fox, T.; Linden, A.; Nevado, C. *Angew. Chem. Int. Ed.* **2017**, *56*, 12862–12865.
- (15) Kumar, R.; Linden, A.; Nevado, C. *Angew. Chem. Int. Ed.* **2015**, *54*, 14287–14290.
- (16) David, B.; Monkowius, U.; Rust, J.; Lehmann, C. W.; Hyzak, L.; Mohr, F. *Dalton Trans.* **2014**, *43*, 11059–11066.
- (17) Rocchigiani, L.; Fernandez-Cestau, J.; Budzelaar, P. H. M.; Bochmann, M. *Chem. Commun.* **2017**, *53*, 4358–4361.
- (18) Reviews: (a) Bronner, C.; Wenger, O. S. *Dalton Trans.* **2011**, *40*, 12409–12420. (b) Wong, K. M.-C.; Chan, M. M.Y.; Yam, V. W.-W. *Adv. Mater.* **2014**, *26*, 5558–5568.
- (19) Complex **4** has been independently identified as one of the products in the reaction of **1** with an excess of L-selectride: C. Nevado, personal communication.
- (20) (a) Hrobárik, P.; Hrobáriková, V.; Meier, F.; Repický, M.; Komarovský, S.; Kaupp, M. *J. Phys. Chem. A* **2011**, *115*, 5654–5659. (b) Hrobárik, P.; Hrobáriková, V.; Greif, A.; Kaupp, M. *Angew. Chem. Int. Ed.* **2012**, *51*, 10884–10888. (c) Greif, A. H.; Hrobárik, P.; Hrobáriková, V.; Arbuznikov, A. V.; Autschbach, J.; Kaupp, M. *Inorg. Chem.* **2015**, *54*, 7199–7208.
- (21) Greif, A. H.; Hrobárik, P.; Kaupp, M. *Chem. Eur. J.* **2017**, *23*, 9790–9803.
- (22) For SO-induced shielding/deshielding effects on ¹³C shifts in gold complexes, see also: (a) Vicha, J.; Foroutan-Nejad, C.; Pawlak, T.; Munzarová, M.; Straka, M.; Marek, R. *J. Chem. Theory Comput.* **2015**, *11*, 1509–1517. (b) Novotný, J.; Vicha, J.; Bora, P. L.; Repický, M.; Straka, M.; Komarovský, S.; Marek, R. *J. Chem. Theory Comput.* **2017**, *13*, 3586–3601.
- (23) Roşca, D.-A.; Fernandez-Cestau, J.; Hughes, D. L.; Bochmann, M. *Organometallics* **2015**, *34*, 2098–2101.
- (24) Nijamudheen, A.; Karmakar, S.; Datta, A. *Chem. Eur. J.* **2014**, *20*, 14650–14658.
- (25) Estes, D. P.; Norton, J. R.; Jockusch, S.; Wesley Sattler, W. *J. Am. Chem. Soc.* **2012**, *134*, 15512–15518.
- (26) (a) Matsuura, K.; Muto, H. *J. Phys. Chem.* **1993**, *97*, 8842–8844. (b) Huang, M.-B.; Liu, Y. *J. Phys. Chem. A* **2001**, *105*, 923–929.
- (27) Clark, H. C.; Ferguson, G.; Goel, A. B.; Janzen, E. G.; Ruegger, H.; Siew, P. Y.; Wong, C. S. *J. Am. Chem. Soc.* **1986**, *108*, 6961–6972.
- (28) Lancaster, S. J.; Rodriguez, A.; Lara-Sanchez, A.; Hannant, M. D.; Walker, D. A.; Hughes, D. L.; Bochmann, M. *Organometallics* **2002**, *21*, 451–453.
- (29) (a) Currie, L.; Rocchigiani, L.; Hughes, D. L.; Bochmann, M. *Dalton Trans.* **2018**, *47*, 6333–6343. (b) Rocchigiani, L.; Fernandez-Cestau, J.; Budzelaar, P. H. M.; Bochmann, M. *Chem. Eur. J.* **2018**, DOI: 10.1002/chem.201801277.
- (30) Rocchigiani, L.; Fernandez-Cestau, J.; Agonigi, G.; Chambrier, I.; Budzelaar, P. H. M.; Bochmann, M. *Angew. Chem. Int. Ed.* **2017**, *56*, 13861–13865.

(31) Note that ^1H hydride shifts computed at the two-component quasi-relativistic 2c-ZORA(SO)/PBE0-XC level, including the previously neglected terms from the exchange-correlation (XC) response kernel (see refs. 20c and 32), agree very well with those obtained using the four-component fully relativistic (mDKS) method along with the same hybrid functional (cf. Table 1).

(32) (a) Autschbach, J. *Mol. Phys.* **2013**, *111*, 2544–2554. (b) Greif, A. H.; Hrobárik, P.; Autschbach, J.; Kaupp, M. *Phys. Chem. Chem. Phys.* **2016**, *18*, 30462–30474.

(33) In organic compounds ^1H NMR shifts are often considered to shift downfield (upfield) upon decrease (increase) of the atomic charge at the hydrogen atom.

(34) This is in line with the very recent predictions and detailed analysis of ^1H NMR shifts for hypothetical linear $\text{HAu}^{\text{I}}\text{L}$ hydrides, where the strong *trans* ligands were shown to destabilize the $\sigma(\text{Au}-\text{H})$ -type bonding MOs.²¹ These have a deshielding δ_{SO} contribution and compete with the shielding effect of $\text{Au}(\text{d}_{\pi})$ -based MOs. Once the $\sigma(\text{Au}-\text{H})$ -type bonding MO has moved substantially above $\text{Au}(\text{d}_{\pi})$ -based MOs, mixing of these two types of scalar relativistic MOs into spinors becomes less favorable (the more so, the larger the energy gap between them) and results in an overall δ_{SO} deshielding, and thus positive ^1H hydride shifts.

(35) The remarkable deviations are found for complexes with π -acceptor (CO and PH_3) ligands. This can be attributed to the more pronounced π -back donation ($\text{Au}\rightarrow\text{L}$) in the electron-richer $\text{Au}(\text{I})$ hydrides as compared to $\text{Au}(\text{III})$ congeners.

(36) Despite the tendency of increasing negative charge at the hydride ligand upon increasing the σ -donor strength of the *trans* ligand, no reasonable correlation between atomic charges at the hydride ligand and ^1H NMR shifts for a wide set of ligands can be established.

(37) Useful correlations between ligand NMR shifts and M–L bond covalency, assessed by QTAIM delocalization indices, have been recently demonstrated also for actinide-chalcogen and organothorium complexes: a) Smiles, D. E.; Wu, G.; Hrobárik, P.; Hayton, T. W. *J. Am. Chem. Soc.* **2016**, *138*, 814–825; b) Smiles, D. E.; Wu, G.; Hrobárik, P.; Hayton, T. W. *Organometallics* **2017**, *36*, 4519–4524. In these multiple-bonded f^0 systems, the ligand $^{77}\text{Se}/^{125}\text{Te}/^{13}\text{C}$ shifts are, however, dominated by paramagnetic shielding contribution and the opposite trend was observed, *i.e.* the ligand NMR shifts became more deshielded along with increasing M–L bond covalency.

(38) Miller, W. T., Jr; Sun, K. K. *J. Am. Chem. Soc.* **1970**, *92*, 6985–6987.

(39) (a) Smith, D. A.; Rosca, D.-A.; Bochmann, M. *Organometallics* **2012**, *31*, 5998–6000. (b) Chambrier, I.; Rosca, D.-A.; Fernandez-Cestau, J.; Hughes, D. L.; Budzelaar, P. H. M.; Bochmann, M. *Organometallics*, **2017**, *36*, 1358–1364.

(40) Rosca, D.-A.; Smith, D. A.; Bochmann, M. *Chem. Commun.* **2012**, *48*, 7247 – 7249.

(41) Coles, S. J.; Gale, P. A. *Chem. Sci.* **2012**, *3*, 683–689.

TOC IMAGE

